

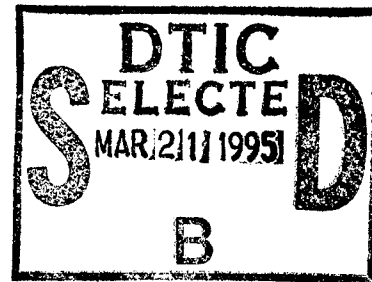
**PL-TR-94-2225**

**REGIONAL SEISMIC EVENT IDENTIFICATION  
AND IMPROVED LOCATIONS WITH  
SMALL ARRAYS**

**Frank L. Vernon  
J. Bernard Minster  
John A. Orcutt**

**University of California  
Scripps Institution of Oceanography  
La Jolla, CA 92093-0210**

**6 July 1994**



**Scientific Report No. 1**

**APPROVED FOR PUBLIC RELEASE; DISTRIBUTION UNLIMITED**



**PHILLIPS LABORATORY  
Directorate of Geophysics  
AIR FORCE MATERIEL COMMAND  
HANSCOM AIR FORCE BASE, MA 01731-3010**

**19950317 149**

**DTIC QUALITY INSPECTED 1**

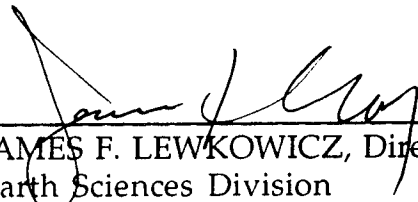
SPONSORED BY  
Advanced Research Projects Agency (DoD)  
Nuclear Monitoring Research Office  
ARPA ORDER NO 128

MONITORED BY  
Phillips Laboratory  
CONTRACT NO. F19628-93-K-0021

The views and conclusions contained in this document are those of the authors and should not be interpreted as representing the official policies, either express or implied, of the Air Force or the U.S. Government.

This technical report has been reviewed and is approved for publication.

  
JAMES F. LEWKOWICZ  
Contract Manager  
Earth Sciences Division

  
JAMES F. LEWKOWICZ, Director  
Earth Sciences Division

This report has been reviewed by the ESC Public Affairs Office (PA) and is releasable to the National Technical Information Service (NTIS).

Qualified requestors may obtain additional copies from the Defense Technical Information Center. All others should apply to the National Technical Information Service.

If your address has changed, or if you wish to be removed from the mailing list, or if the addressee is no longer employed by your organization, please notify PL/TSI, 29 Randolph Road, Hanscom AFB, MA 01731-3010. This will assist us in maintaining a current mailing list.

Do not return copies of this report unless contractual obligations or notices on a specific document requires that it be returned.

REPORT DOCUMENTATION PAGE			Form Approved OMB No. 0704-0188	
Public reporting burden for this collection of information is estimated to average 1 hour per response, including the time for reviewing instructions, searching existing data sources, gathering and maintaining the data needed, and completing and reviewing the collection of information. Send comments regarding this burden estimate or any other aspect of this collection of information, including suggestions for reducing this burden, to Washington Headquarters Services, Directorate for Information Operations and Reports, 1215 Jefferson Davis Highway, Suite 1204, Arlington, VA 22202-4302, and to the Office of Management and Budget, Paperwork Reduction Project (0704-0188), Washington, DC 20503.				
1. AGENCY USE ONLY (Leave blank)		2. REPORT DATE 6 July 1994		3. REPORT TYPE AND DATES COVERED Scientific No. 1
4. TITLE AND SUBTITLE Regional Seismic Event Identification and Improved Locations With Small Arrays			5. FUNDING NUMBERS PE 62301E PR NM93 TA GM WU AB Contract F19628-93-K-0021	
6. AUTHOR(S) Frank L. Vernon J. Bernard Minster John A. Orcutt				
7. PERFORMING ORGANIZATION NAME(S) AND ADDRESS(ES) University of California Scripps Institution of Oceanography La Jolla, CA 92093-0210			8. PERFORMING ORGANIZATION REPORT NUMBER	
9. SPONSORING/MONITORING AGENCY NAME(S) AND ADDRESS(ES) Phillips Laboratory 29 Randolph Road Hanscom AFB, MA 01731-3010 Contract:Manager: James Lewkowicz/GPEH			10. SPONSORING/MONITORING AGENCY REPORT NUMBER  PL-TR-94-2225	
11. SUPPLEMENTARY NOTES				
12a. DISTRIBUTION/AVAILABILITY STATEMENT Approved for public release; distribution unlimited			12b. DISTRIBUTION CODE	
13. ABSTRACT (Maximum 200 words) As part of our work in receiver site characterization we have written Kirchhoff migration software that can be used to process small-aperture 3-component array recordings of regional earthquakes and explosions to develop images of sub- and free-surface scatterers. Essentially, the software back-projects coda energy from the recording stations into the crust from which it propagated after suppressing the primary energy. If the crustal volume contains scatterers that were excited by the primary events and these scattered phases were detected by the sensor array, this energy is collapsed in space by the migration onto the scattering loci. Although most sensor array's offer limited aperture, and thus limited spatial resolution, by considering a broadly distributed event array we can take advantage of the synthetic aperture and increase spatial resolution.  We have applied this type of processing to synthetics to gauge imaging resolution. We have examined local events recorded by the Pinon Flat Broadband Array (PFBA) and used 3-Component backprojection to image a deeply buried scatterer in the vicinity of the San Andreas Fault at Moho depth. We are currently assessing the feasibility of using this software to refine regional shallow-source depth estimates.				
14. SUBJECT TERMS  Site Characterization, Kirchhoff Migration, Backprojection, Imaging Resolution, Scatterer			15. NUMBER OF PAGES 32	
			16. PRICE CODE	
17. SECURITY CLASSIFICATION OF REPORT Unclassified		18. SECURITY CLASSIFICATION OF THIS PAGE Unclassified		19. SECURITY CLASSIFICATION OF ABSTRACT Unclassified
				20. LIMITATION OF ABSTRACT SAR

## CONTENTS

1.	Task Objectives.	1
2.	Technical Problem	2
	2.1 Imaging Prominent Scatterers	2
	2.2 Small-Event Discrimination	2
3.	General Methodology	2
	3.1 Imaging Prominent Scatterers	2
	3.2 Small-Event Discrimination	3
4.	Technical Results	3
	4.1 Imaging Prominent Scatterers - The Technique	3
	4.2 Spatial Resolution	5
	4.3 Teleseismic Excitation of Crustal Scatterers - An Illustration of the Technique	7
	4.3.1 Resolving Buried Scatterers - Analysis of Synthetics	7
	4.4 Imaging Buried Sources Excited by Regional Events in a Vertically Varying Earth	10
	4.4.1 Spatial Resolution	10
	4.4.2 Recorded Data	15
	4.5 Depth Determination	21
	4.6 The IMS Project	21
5.	Important Findings and Conclusions	21
6.	Significant Hardware Development	22
7.	Implications for Further Research	22
8.	References	22

<b>Accession For</b>	
NTIS GRA&I	<input checked="checked" type="checkbox"/>
DTIC TAB	<input type="checkbox"/>
Unannounced	<input type="checkbox"/>
Justification	
By	
Distribution/	
Availability Codes	
Dist	Avail and/or Special
A-1	

## 1. TASK OBJECTIVES

There are three broad objectives in this research effort. The first two involve the analysis of seismic array data to improve the accuracy of regional event locations and to develop better methods for depth estimation. The third objective is to develop automated techniques for the identification of ripple-fired quarry blasts.

Specifically, the work statement includes the following:

- Extending our *beam-stack* imaging technique to examine crustal scatterers near seismic arrays by (1) combining array processing and analysis of 3-Component seismograms, (2) keeping the phase information through horizontal *migration* of the scattered wavefields, (3) generalizing the technique to permit scanning full crustal volumes for scatterers, and (4) analyzing high-frequency local and regional events as well as teleseisms.
- Using 3-Component data from four different arrays to (1) develop a quantitative statistical description of the variability of wave vector estimates with local emplacement, (2) look for crustal phases (reverberations) that are sensitive to the depth of regional sources. We will support the interpretations with finite difference and phase screen forward modeling of synthetic seismograms.
- Extending whole seismogram interpretation techniques aimed at identifying ripple-fired quarry blasts. We will (1) apply our *sonogram* technique to new array data, including 3-Component arrays, (2) develop and test improvements to the current strategy, which relies on the *binarization* of the sonograms, by use of the statistics of zero-crossings, and (3) reduce the procedure to the test of a single quantity, by generalizing the statistics of extreme values of 2-D cepstra.
- Incorporating source identification and location algorithms developed as a result of our research into the IMS.

## 2. TECHNICAL PROBLEM

### 2.1 Imaging Prominent Scatterers

An important aspect of seismic monitoring is to understand the generation of seismic coda, particularly the near-station mechanisms. Numerous studies (*e.g.* Aki, 1969; Aki & Chouet, 1975) have argued that coda waves generated in the continental crust are most likely due to scattering by inhomogeneities. Although studies quantifying the effects of scattering have mostly been statistical and have dealt with the influence of small-scale random scatterers, some deterministic studies (Key, 1967; Key, 1968; Gupta *et al.*, 1990; Gupta, Lynnes & Wagner, 1990; Bannister, Husebye & Ruud, 1990; Lay, 1987; Lynnes & Lay, 1989) have produced compelling evidence that large crustal inhomogeneities or topographic features are capable of producing significant amounts of scattered energy, principally in the form of large, identifiable seismic phases, which affect nuclear monitoring and discrimination. These prominent scattered phases may be confused with direct arrivals (for example free-surface reflections used as “depth phases”) - particularly if they are detected by single sensors. Being able to identify these “secondary” sources and anticipate the scattered phases they produce is the first step toward being able to reduce this confusion. Although numerous studies (*e.g.* Key, 1967; Gupta *et al.*, 1990) have concluded that the most significant sources of identifiable phases are associated with free-surface topography, recent work by Dr. S.A. Magnier, at IGPP, concluded that buried scatterers excited by regional events were contributing identifiable seismic phases to seismic coda in the vicinity of the Cecil and Ida Green Piñon Flat Geophysical Observatory (PFO) in southern California.

### 2.2 Small-event Discrimination

A second challenge to the seismic monitoring community has arisen due to recent interest in negotiating a Comprehensive Test Ban Treaty (CTBT) with the Former Soviet Union (FSU). As discussed by Stump *et al.* (1988), a reduced Threshold Test Ban Treaty would bring the magnitude of the largest allowable nuclear explosions down to that of large “engineering” explosions otherwise known as quarry blasts. Such a treaty requires an ability to discriminate small, common, natural or man-made seismic events from buried nuclear explosions - particularly buried, decoupled, events with body wave magnitudes,  $m_b$ , as low as 2.5 (Wallace *et al.*, 1992). The most popular quarry blasting technique is “ripple-firing” - a process in which a large number of spatially deployed charges are detonated in sequence to enhance fracturing of the rock.

## 3. GENERAL METHODOLOGY

### 3.1 Imaging Prominent Scatterers

It has been demonstrated that prominent buried and unburied scatterers near the receiver and source can give rise to late, high-amplitude, phases. Very similar phases can be produced by free-surface

bounces. To attempt to reduce possible confusion regarding the origin of late arriving phases we have developed a technique that uses 3-Component (3-C) array recordings of local, regional and teleseismic events to locate and image the point(s) of origin of the prominent late arriving phases. The technique is capable of imaging scatterers located at the Earth's surface or within a volume of the crust located in the vicinity of the array. The algorithm back-projects the array recordings, after suppressing energy that has arrived directly from the original source, through a layered crust to the local points of origin. Our technique takes advantage of 3-C array data by simultaneously performing beamforming and polarization analyses to look for scatterers generating a particular type of particle motion. This allows us to look specifically for local sources of surface waves or buried sources of shear or compressional energy. We analyze infinitesimal synthetic scatterers to gauge spatial resolution when recordings are made by 1-C and 3-C arrays, and to get some idea of how a point scatterer might become distorted when viewed in this manner. An analysis of recorded data, made by the PFBA 3-C broadband small-aperture array in southern California follows.

### **3.2 Small-event Discrimination**

Considering the great number of seismic events that need to be considered to monitor a CTBT and the frequency of ripple-fired chemical blasting at small magnitude levels (*Richards, Anderson & Simpson, 1992*) we have developed a technique that automatically discriminates small ripple-fired chemical blasts from Earthquakes and single-event explosions (*Hedlin, Minster & Orcutt, 1989; Hedlin, Minster & Orcutt, 1990*). The technique examines the manner in which the spectral composition of the recorded signal varies with time. In theory we expect that ripple-fired mining events should yield seismic coda with a spectral signature that is relatively invariant with passing time. Simpler events (*e.g.* nuclear explosions) should give rise to seismic coda that is much less structured in time and frequency. The development phase of this project is complete and the algorithm has been automated so that it can deal with the large volumes of events we expect in an area of interest at small magnitude ranges. We are currently implementing this software as a module of the Intelligent Monitoring System (IMS).

## **4. TECHNICAL RESULTS**

### **4.1 Imaging Prominent Scatterers -The Technique**

We (*Hedlin, Minster & Orcutt, 1991*) developed a systematic technique to image nearby large scatterers at the free surface or within a crustal volume near a seismic array. Since the problem of imaging sources of scattered energy using two-dimensional (2-D) array records is akin to the use of 1-D seismic reflection profiles to produce images of subsurface velocity contrasts, we relied on the experience of the reflection seismology community in that initial analysis. The underlying premise of our technique is that at least some of the teleseismic coda energy is generated by local scatterers. We consider each scatterer as a secondary source which is excited with a delay estimated from elementary ray theory. Given an array recording of the scattered waves, enough information exists to locate and image this

secondary source using a modified beamforming technique.

As described by *Hedlin, Minster & Orcutt* (1994) the spherical wavefronts produced by a point scatterer in a homogeneous medium have hyperbolic moveout when recorded in time by a spatial array. Given this simple situation, to achieve the greatest enhancement of seismic motions caused by this scatterer (at the expense of motions caused by scatterers at other locations), and thus to achieve the best image of the scatterer itself, we sum the motions recorded by the sensors after reversing the hyperbolic moveout to bring the traces into proper alignment (*i.e.* we remove the curvature in the scattered wavefront). We image the local scatterers in an area (or volume) of interest by systematically scanning for secondary sources at all discrete locations. This imaging approach is a simple extension of the hyperbola summation migration method (*Yilmaz*, 1987) in seismic reflection and, because of its 2-D nature, is referred to hereafter as hyperboloid summation migration. Since a delay-and-sum operation is involved, this method is akin to standard beamforming and bears some resemblance to  $f$ - $\mathbf{k}$  analysis. This technique is distinguished, however, by its cognizance of not only the wavenumber but also the onset time of a seismic arrival. As a result, the technique can be used to infer the likely spatial location of the secondary source. This method differs from previous attempts to locate large near-receiver scatterers since it is capable of accommodating simultaneously many primary events from different azimuths to give a balanced, redundant illumination of local scatterers while suppressing the influence of near-source scatterers. By adjusting the assumed velocity of scattered waves, we can easily accommodate secondary sources located at any point in the crust.

Although it is easy to predict, and compensate for, moveout we do not know when a scatterer might have been illuminated (because the incident wavetrain is not generally impulsive). As a result it is not obvious where to look for a scattered phase arising from a particular location in the stack (beam). By necessity we relate all times to the primary wave onset time at the center of the array,  $t_i$ , which is easily determined by examining the array records. The arrival time of the scattered wave at the center of the array,  $t_s$ , is given by:

$$t_s = t_i + \Delta + \tau \quad (1)$$

where  $\Delta$  is the time delay, at the center of the array, that separates the primary wave onset phase from the phase that excited the scatterer (the parent phase). The time delay between the arrival of the parent phase and the scattered phase is represented by  $\tau$ . When the Earth model is homogeneous and the primary source is distant we can show that, for a single hypothetical scatterer,  $\tau$  is given by:

$$\tau = \mathbf{R}_{AS} \cdot (\mathbf{p}_i - \mathbf{p}_s) \quad (2)$$

where  $\mathbf{p}_i$  is the vector slownesses of the parent phase and  $\mathbf{R}_{AS}$  is the spatial vector connecting the center



of the array to the hypothetical scatterer. It is possible to estimate  $\mathbf{p}_s$  by considering a suite of broadly distributed events and computing a number of preliminary images while varying this parameter and selecting the value that brings the image into the sharpest focus. The slowness of the incident energy,  $\mathbf{p}_i$ , is well constrained by fitting a least-squares best fit plane (in  $x$ - $y$ - $t$  space) to the first breaks on the array records. To increase image stability we convert the beams to envelopes and convolve the envelopes with boxcar functions (typically 1 to 5 s long). To suppress the energy coming directly from the primary source we coherently subtract the primary source beam from the individual channels prior to stacking (beam correction).

To accommodate 3-C array data we rotate each individual station prior to migration to look for a particular type of particle motion arriving from a specified crustal location. To accommodate primary events and scatterers buried within a vertically varying Earth we connect the scatterers, receivers and primary events with rays shot through a 1-dimensional velocity model. Raytracing provides enough information to guide the beamforming and polarization analyses and relates all occurrences in time.

#### 4.2 Spatial Resolution

A parameter central to the understanding of spatial resolution is the time delay that exists between arrivals of the incident (parent) and the secondary (scattered) phases at the array. To illustrate this point we consider an array and a single scatterer both located at the surface of a homogeneous Earth receiving waves from a teleseism located directly beneath. It is easy to see that a circle passing through the scatterer, centered at the array, describes all possible surface locations which have the same time delay as the scatterer. By manipulation of equation (2) it can be shown that, in general, locations which have a common delay time  $\tau$  lie on a surface described by:

$$|\mathbf{R}_{as}| = \tau / [|\mathbf{p}_s| - |\mathbf{p}_i| \cos(\theta)] \quad (3)$$

where  $\theta$  is the angle between the vectors pointing from the array to the primary source and to the scatterer. When  $\mathbf{p}_s$  is greater than  $\mathbf{p}_i$  (e.g. P to  $R_g$  or P to S scattering) this describes an ellipsoid of revolution with one focus at the center of the array, major axis pointing to the primary source and eccentricity equal to  $|\mathbf{p}_i| / |\mathbf{p}_s|$ . The circle described above is simply the trace of a vertically oriented ellipsoid on the horizontal plane. When the primary source is not directly beneath, the ellipsoid tilts from the vertical and the time-delay curve on the free-surface becomes elliptical. When the incident and scattered wave velocities are equal (e.g. P to P scattering) the eccentricity equals 1 and the surface is a paraboloid of revolution.

This observation is important because the manner in which time delay surface appears in the plane, or volume, being imaged determines the resolution of point scatterers and allows us to predict how scatterers that might be symmetrical might become distorted in the image. If two scatterers lie on the same

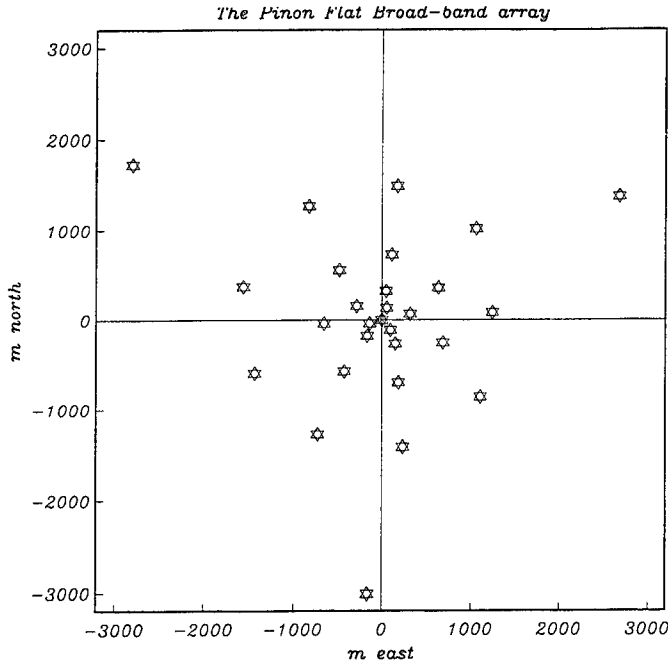


**Figure 1:** The Piñon Flat Broad-band array (PFBA). This 28 element 6 km aperture array was deployed for 3 months in early 1991. Each element consists of 3 orthogonal STS-2 sensors (.0083 to 40 Hz).

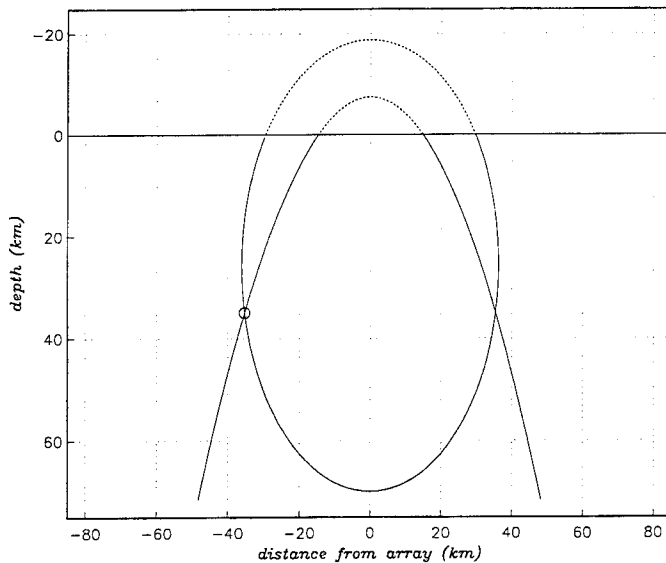


**Figure 2:** Constant time delay curves passing through a scatterer located 35 km from an array at a depth of 35 km. The scatterer is located in a homogeneous volume and thus the time delay curves are an ellipse (P to S scattering) and a parabola (P to P). The scatterer is excited by a teleseismic arrival with infinite phase velocity.

time-delay surface it will be relatively difficult to resolve them since, by definition of the curve, their seismic offspring will arrive at the array at the same time. Resolution along constant time-delay surfaces will be relatively poor and will be determined by the rate at which the slowness of scattered waves changes along the constant time-delay curves. If the slowness of scattered waves recorded at the array happens to be invariant for all scatterers on the same time delay surface, we would have no ability to resolve any of the individual scatterers. If, as is often the case, the slowness is slowly varying along a time-delay curve the resolution will likely be poor, and directly proportional to the aperture of the array. Resolution along paths orthogonal to the time-delay surfaces is determined by the temporal resolution of the scattered wave sources. As we (Hedlin, Minster & Orcutt, 1994) found in our analysis of teleseismic signals because of the protracted nature of the incident wavetrains it was necessary to perform deconvolution of the seismic recordings prior to imaging to compact the signal in time and obtain acceptable time-resolution. As we will see, in our analysis of small, local and regional events, the short source times involved preclude the necessity of this additional processing.

When scatterers are located in an inhomogeneous medium the surfaces of constant time-delay deviate from simple surfaces just considered. This complication will be considered in section 4.4. With these observations in mind in the following dis

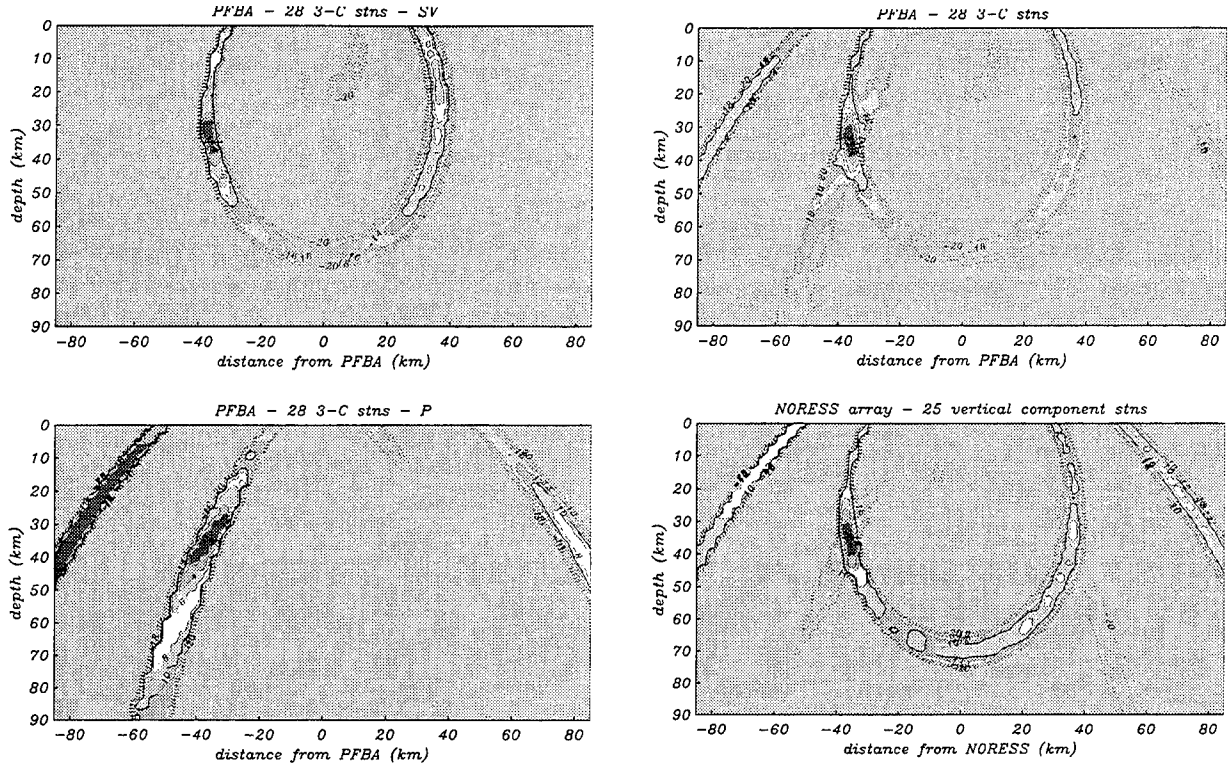


**Figure 3:** (On the left) A synthetic point source of P and SV/SH energy was placed at the location considered in Figure 2. Synthetics were calculated individually for each sensor in the array. In the upper figure the imaging algorithm is seeking P to SV scatterers in a vertical plane passing through the synthetic scatterer. A significant amount of energy is dispersed along the elliptical constant time-delay-curve. The energy near the array is due to P propagating from the scatterer. In the lower figure the algorithm is seeking sources of P excited by incoming P. A significant amount of energy, due to SV produced by the scatterer, is being improperly placed at shallow depths. Additional energy is placed along the parabolic curve passing through the scatter.

**Figure 4:** (On the right) Images calculated by simultaneously seeking P and SV energy detected by the PFBA (top) and NORESS (bottom). The 3-Component PFBA is capable of much higher resolution.

cussion we will make repeated reference to slowness- (along time-delay curve) and time-resolution.

#### 4. 3 Teleseismic Excitation of Crustal Scatterers - An Illustration of the Technique.

Although this contract is mainly concerned with regional event locations it seems appropriate to begin this discussion with an analysis of teleseismic excitation of local scatterers in a homogeneous crust. This scenario is relatively simple and can be used to illustrate the concepts important to understanding the regional problem. The simplicity is due to planar-incident and spherical-scattered wavefronts.

**4.3.1 Resolving Buried Scatterers - Analysis of Synthetics.** To gauge imaging resolution we will consider a buried scatterer excited by a vertically incident impulsive teleseismic P wave. Both the incident and scattered wavefields are recorded by a small-aperture 3-C array deployed at the free-surface. The array geometry is taken from the 28 element PFBA array deployed at the Piñon Flat Observatory (PFO) in 1991 (Figure 1). Using Wavenumber Integration (Apsel and Luco, 1983; Luco and Apsel, 1983) we

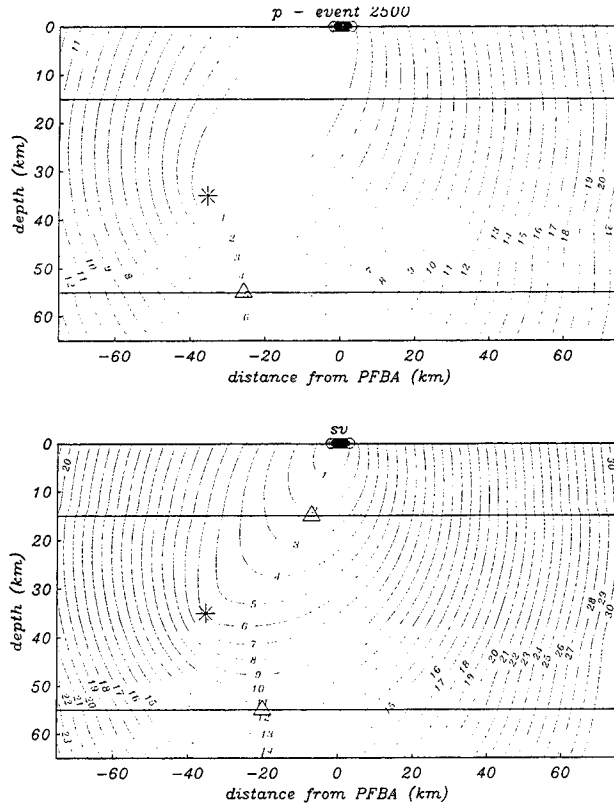


**Figure 5:** Constant time delay surfaces for an Earth consisting of 2 homogeneous layers overlying a half-space. In both figures a primary source is represented by a star and energy bounce, or conversion, points are identified by the triangles. The circles at the top represent the sensors in the array. In the upper figure we consider P to SV scattering. In the lower figure we con-

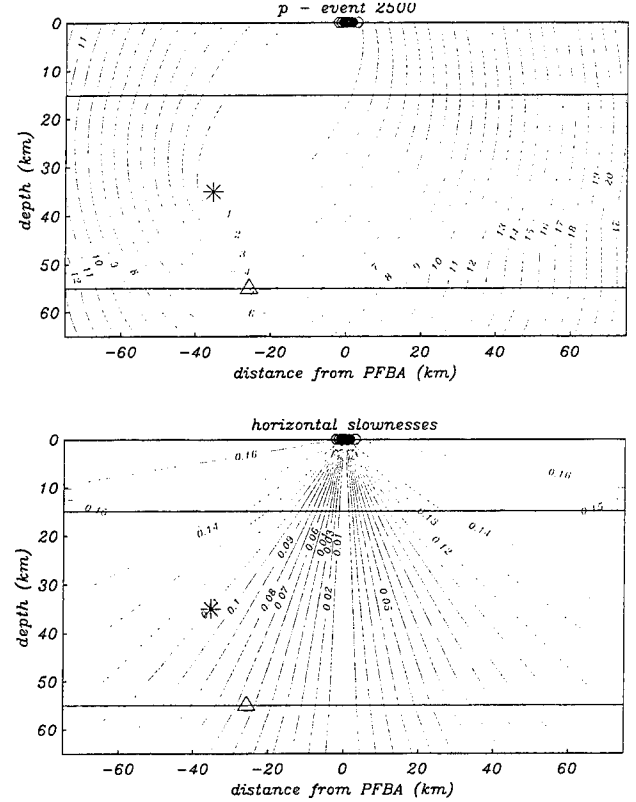


**Figure 6:** The upper half of this figure repeats that presented in the upper half of Figure 5. In the lower figure we display the horizontal slowness expected for P to P scattered phases.

place a point source of compressional and shear energy at 35 km depth, 35 km laterally from the array and calculate synthetics individually for each station in the array. As illustrated in Figure 2 the constant time-delay curves for the P and SV scattered waves caused by the vertically incident teleseism are the ellipse and parabola respectively. As illustrated in Figure 3 (top), when we look for vertically polarized scattered energy we place most of it at the correct location but the slowness-resolution is quite poor. In addition, a small amount of energy is placed just beneath the array (at a depth of 20 km). This is due to unsuppressed P wave energy. Steering for radially polarized energy, Figure 3 (bottom), we again backproject the P wave energy to the correct location however a significant amount of energy is dispersed along the constant delay time parabola. Although through the use of array and polarization processing the algorithm is seeking P to P scattered energy it is not completely suppressing the SV energy produced by the synthetic scatterer and is improperly backprojecting this energy to shallow depths. It is difficult for the array to distinguish between a deep source or SV and a shallow source of P. Similarly, P wave images of shallow P/SV scatterers are contaminated by the SV energy.

This weakness can be remedied, somewhat, by simultaneously seeking P and SV scatterers. By doing

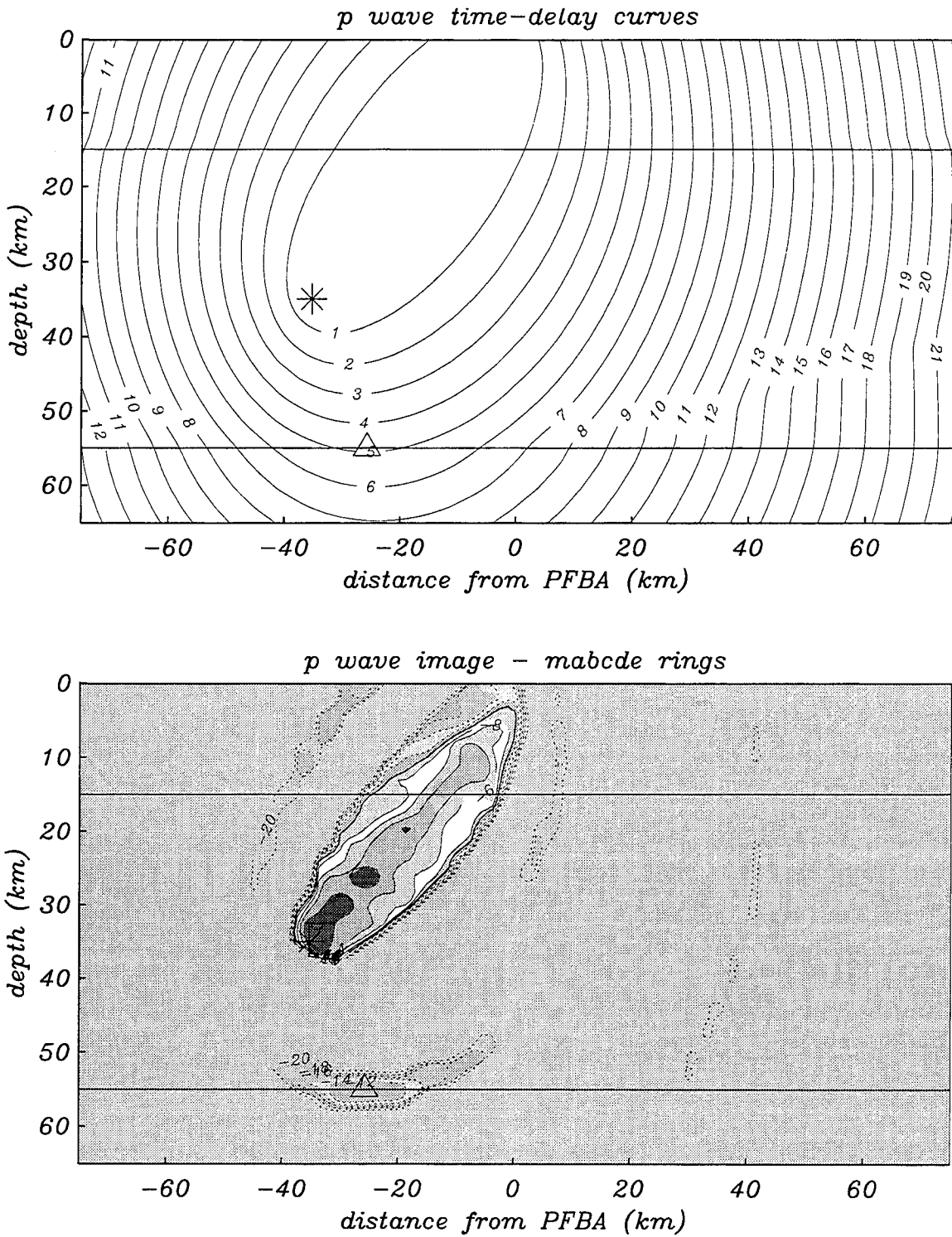


**Figure 7:** The lower half of this figure displays the image calculated using the full (28 element) PFBA. A considerable amount of energy lies within 1 s of the onset - this is due to uncorrected primary energy. The P to P bounce energy is correctly placed on the lower interface. Other energy in the figure is due to unsuppressed P-SV scattering.

so we will stack energy dispersed along parabolic and elliptical curves. In Figure 4 (top) we see that this approach yields a much more highly resolved view of the scatterer. In the lower half of the figure we see that if we are limited to single component data (in this case the NORESS array) that resolution

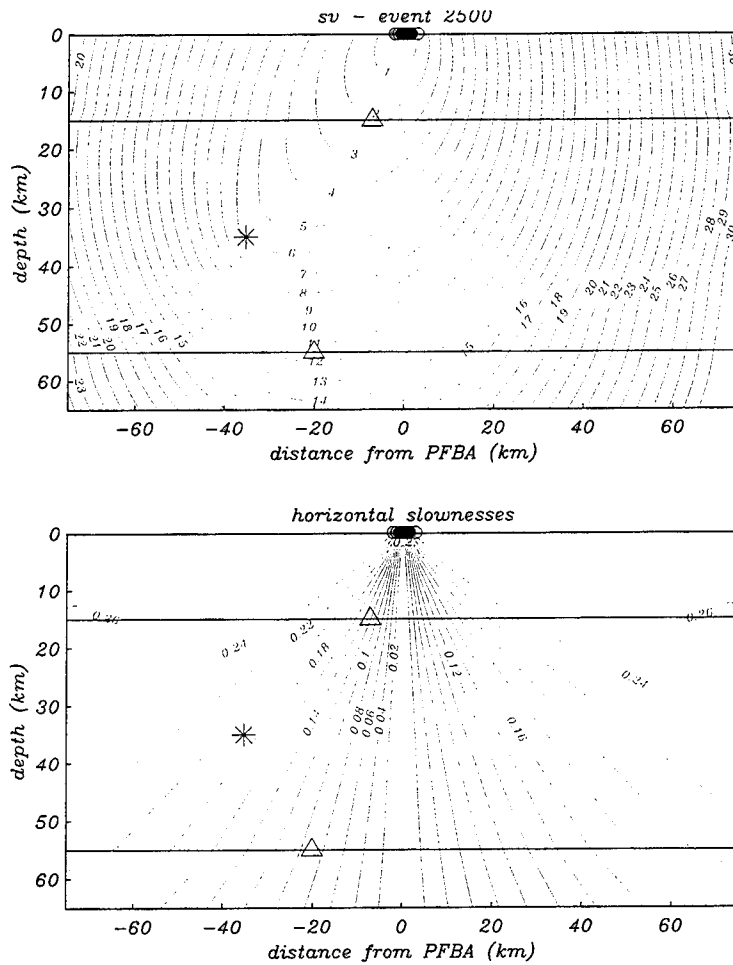


**Figure 8:** The upper half of this figure repeats that presented in the lower half of Figure 5. In the lower figure we display the horizontal slowness expected for P to SV scattered phases arising from the Earth model.

Calculating the Earth's response to this point explosion within a small aperture at the surface (at the PFBA array) we use only a limited number of ray paths. The points at which the recorded energy converts (reflects/transmits) can serve as buried point scatterers. Therefore, we have proposed a simulation in a vertically inhomogeneous medium that can allow us to test the ability of our technique to image scatterers located in a layered crust and excited by a regional event. We can also use the technique to compare 3-C with single (vertical) component arrays and compare different 3-C array geometries. In Figure 5 we display the time delay curves for P to P (top) and P to SV (bottom) scattering. The model consists of a two layer crust over a high velocity half-space. The layer boundaries are indicated by the horizontal lines. The triangles in these figures indicate the points at which the conversions recorded by the array occur. The star reveals the location of the primary event. The conversions occur where the time delay curves become tangent to the interfaces - this corresponds to the point at which the time delay is a minimum (*i.e.* Fermat's principle is obeyed). These curves are the projection of 3-dimensional ellipsoidal (P to SV) or parabolic (P to P) surfaces on to the cross-section. As discussed above, in a homogenous model, the constant time-delay surfaces are ellipsoids or paraboloids of

is, for the most part, worse. A further gain in resolution can be obtained provided that the scatterer is omnidirectional, or we have some notions about the radiation pattern. As shown by *Hedlin, Minster & Orcutt (1994)* by illuminating the local crust with a widely distributed set of primary events we can, in effect, increase the aperture of the array and greatly increase resolution.

#### 4.4 Imaging Buried Sources Excited by Regional Events in a Vertically Varying Earth.

**4.4.1 Spatial Resolution.** To test the resolution of scatterers in a layered Earth we have again calculated and analyzed Wavenumber Integration synthetics. In this simulation, however, the synthetic source (an omnidirectional, impulsive explosion) plays the role of the primary event, not the scatterer (as before) and occurs in a layered Earth.

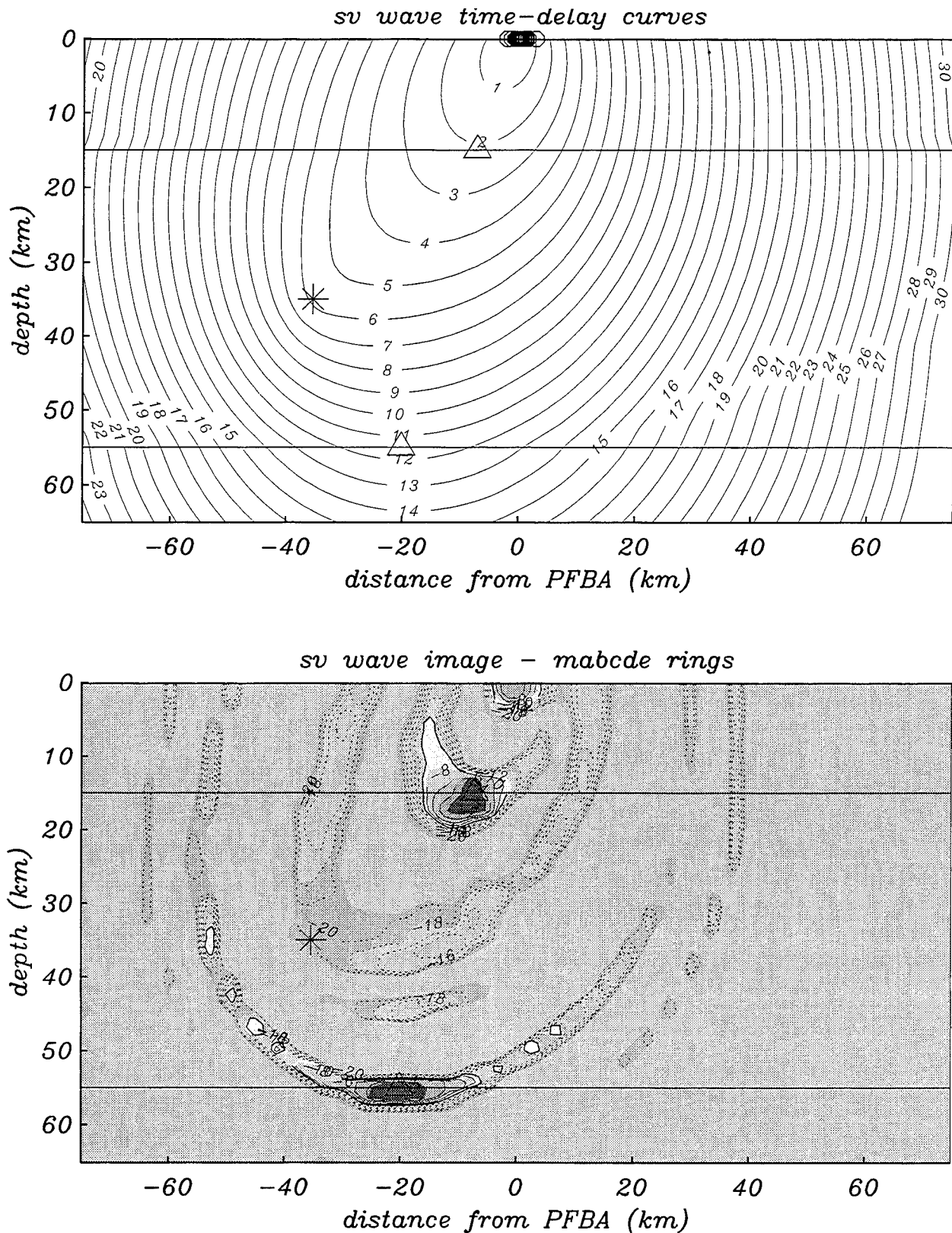


**Figure 9:** The lower half of this figure displays the image calculated using the full (28 element) PFBA. *P* to *SV* conversions at the layer interfaces are imaged, although with limited beam resolution. Other energy in the image is due to unsuppressed *P* to *P* scattering.

revolution which have one focus at the center of the array. In this example, abrupt discontinuities in the time delay-surfaces occur at impedance contrasts. The time-delay surface in a low velocity layer con-



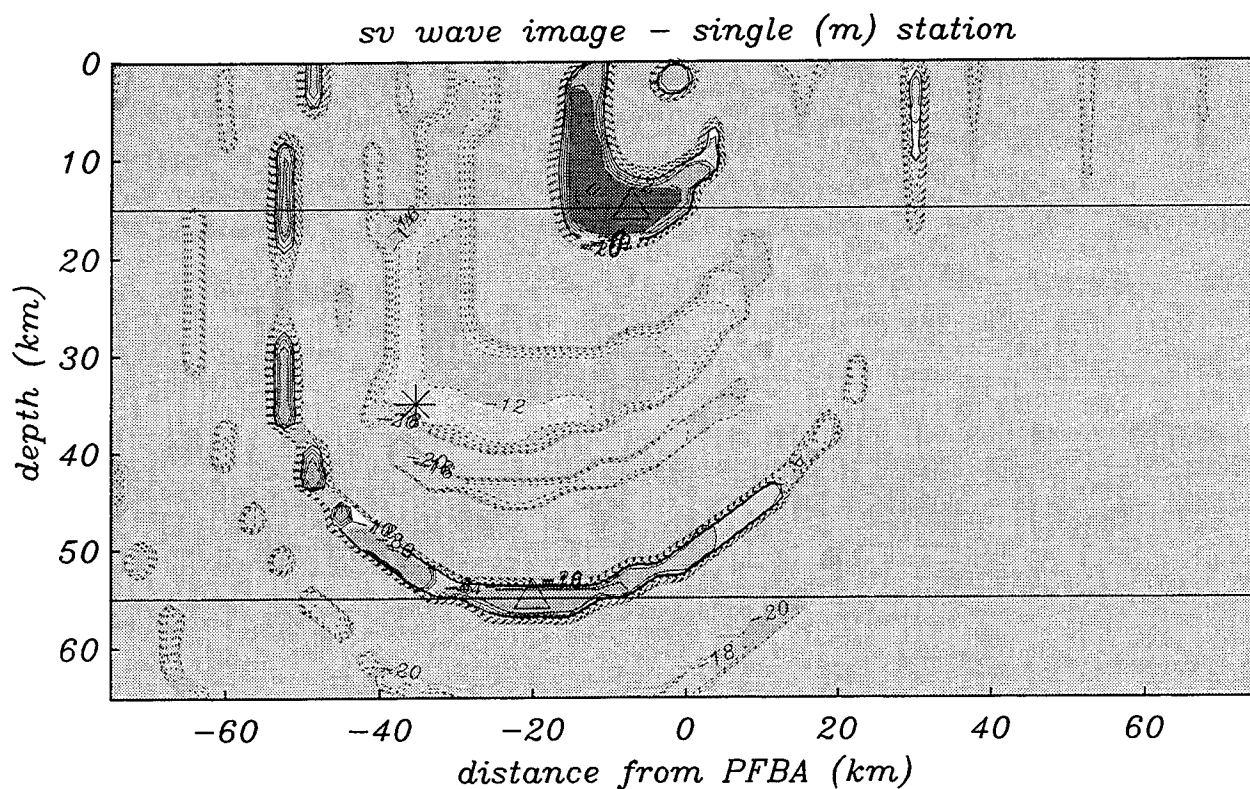
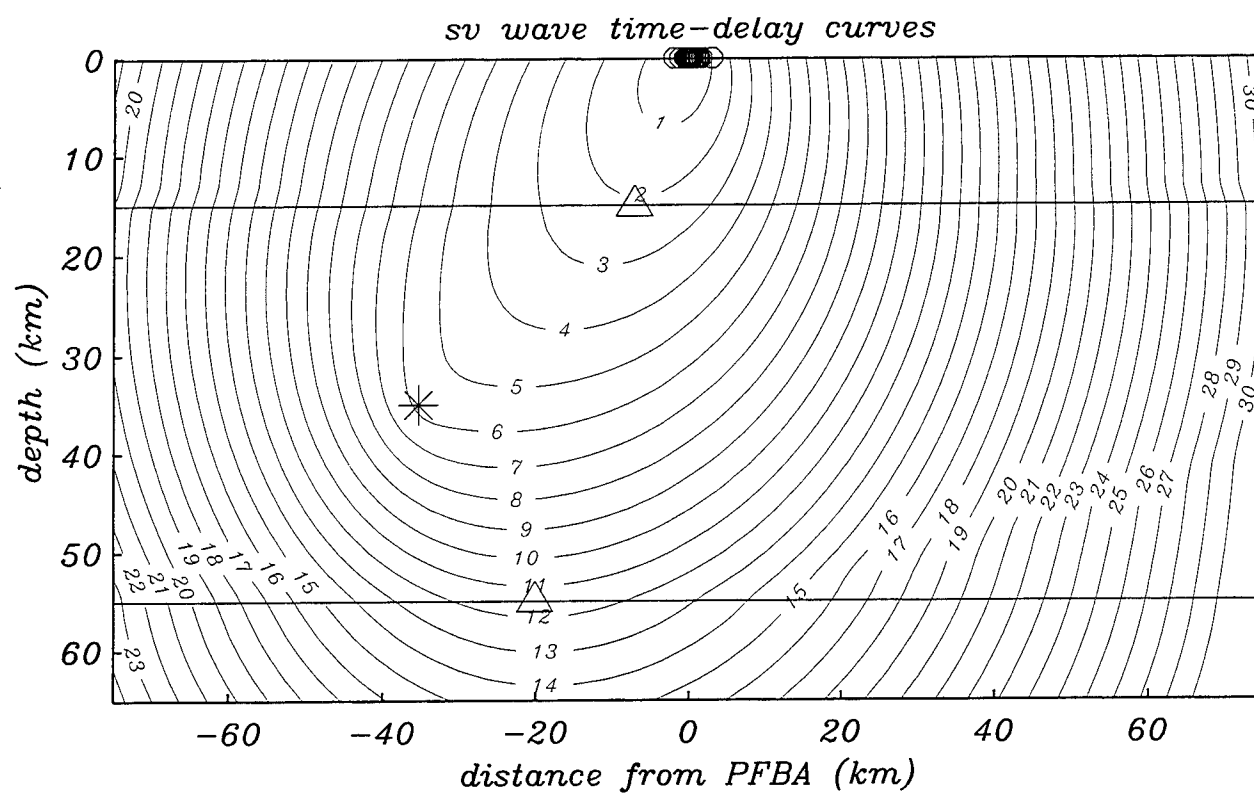


**Figure 10:** This figure is the same as Figure 9 except that only a single 3-C station was used to image scatterers. The beam resolution is relatively poor however the station has correctly placed much of the energy at the interface conversion points.



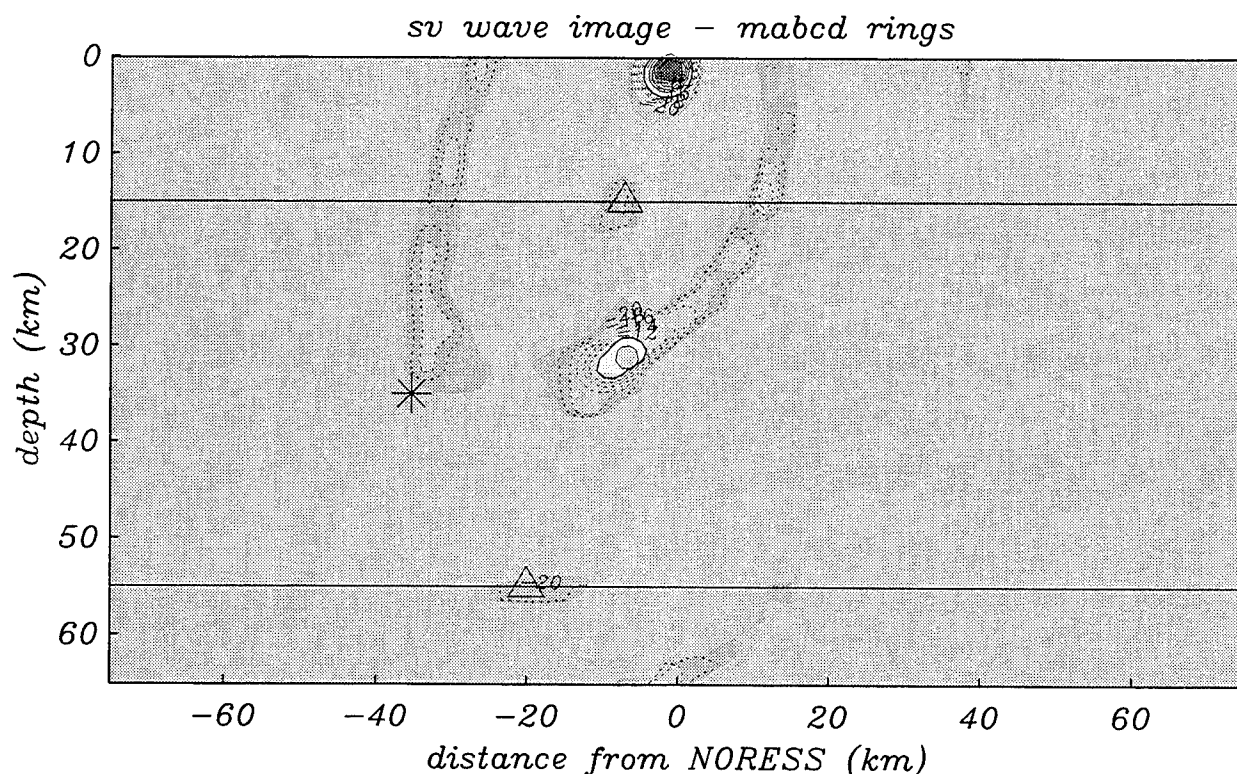
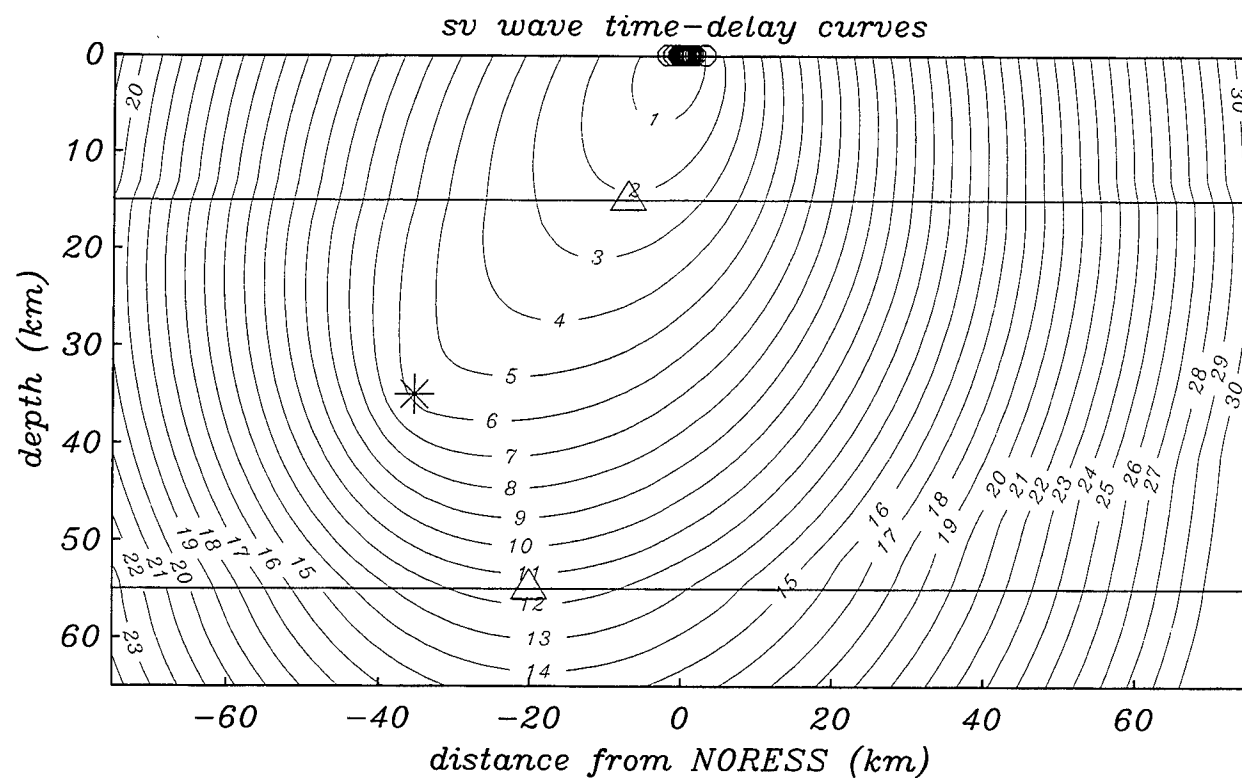


**Figure 11:** Same as Figure 9 except the synthetics were calculated for the NORESS array. This single component array is unable to permit proper back-projection of the energy since particle motion caused by P to SV scattering is largely horizontal. Beam correction has been particularly ineffective.

nects to another surface of lower eccentricity in a neighboring high-velocity layer.

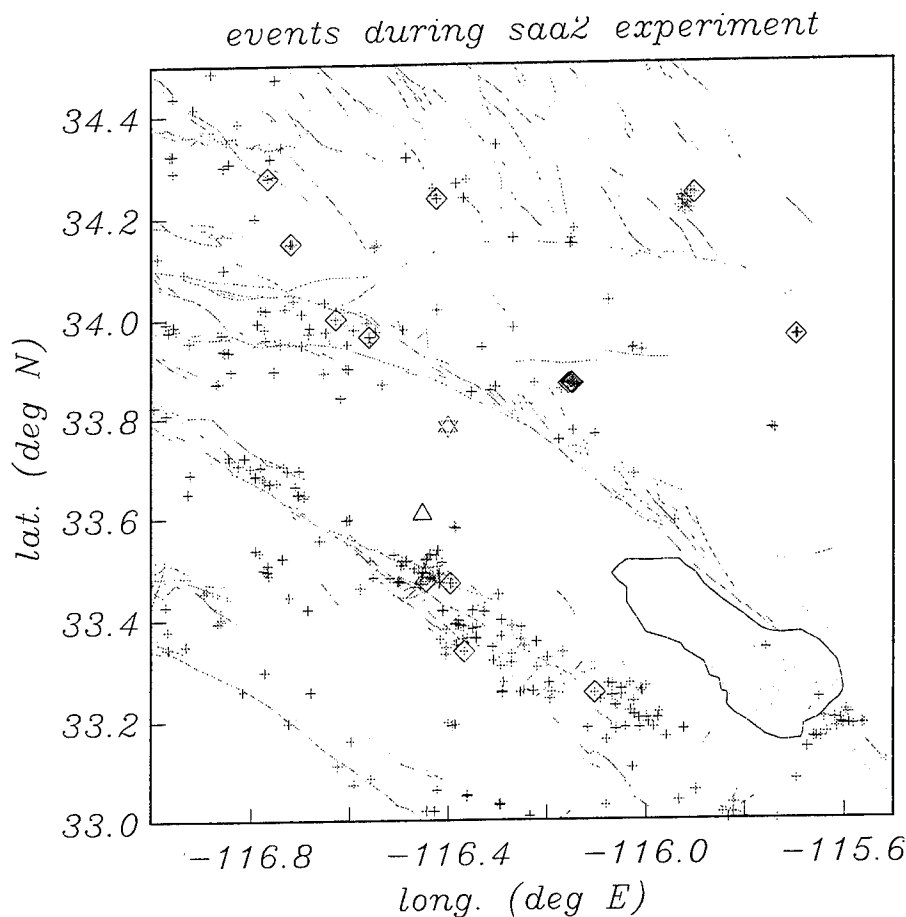


**Figure 12:** Map showing events that occurred during the PFBA experiment. The crosses indicate epicenters of events below  $M_l=2.5$ , the diamonds show events that were larger. Faults are indicated by the faint lines. The array is represented by the black triangle, the scattering location is represented by the star.

The upper figure illustrates that the P-P bounce at the lower interface will arrive at the array roughly 5 s after the direct arrival. From the lower figure we see that the P to SV conversion at the upper interface arrives roughly 2.25 s after the onset. In Figure 6 we consider the P to P scattering. The lower figure shows the slownesses corresponding to the scattered phases. For example, the P-P bounce at the lower interface that arrives 5 s after the direct energy has a slowness of .063 s/km. In Figure 7 we display the P wave image calculated from the synthetics. Clearly the beam suppression is not completely effective. The elliptical smear of energy arriving within 1 s

of the onset is uncorrected direct energy. The beam correction is ineffective because of pronounced amplitude variations across the array. The primary energy is smeared out over a fraction of a second after the onset because of time averaging (in this case 1 s). The P-P reflection at the lower interface (at 55 km) is clearly resolved although with limited slowness-resolution.

Starting with Figure 8 we display the results of processing the same simulation; however, we are now seeking SV scattered energy. The lower half of Figure 8 reveals that P-SV conversions at the upper and lower interfaces should arrive at the array with slownesses of .12 and .09 s/km respectively. The image calculated from this simulation is displayed in Figure 9. The unsuppressed direct energy is located at the array and clearly is insignificant relative to the P-SV conversions. Both are imaged with high time-resolution but rather limited slowness-resolution. The energy that appears in the figure between the ellipses associated with the P-SV conversions arrives roughly 5 s after the direct energy and is due to the P-P bounce at the lower interface. In the regional simulations we see that energy of one type (*e.g.*

91057:06:14:32.500 91057061432 BW: 4.0- 6.0

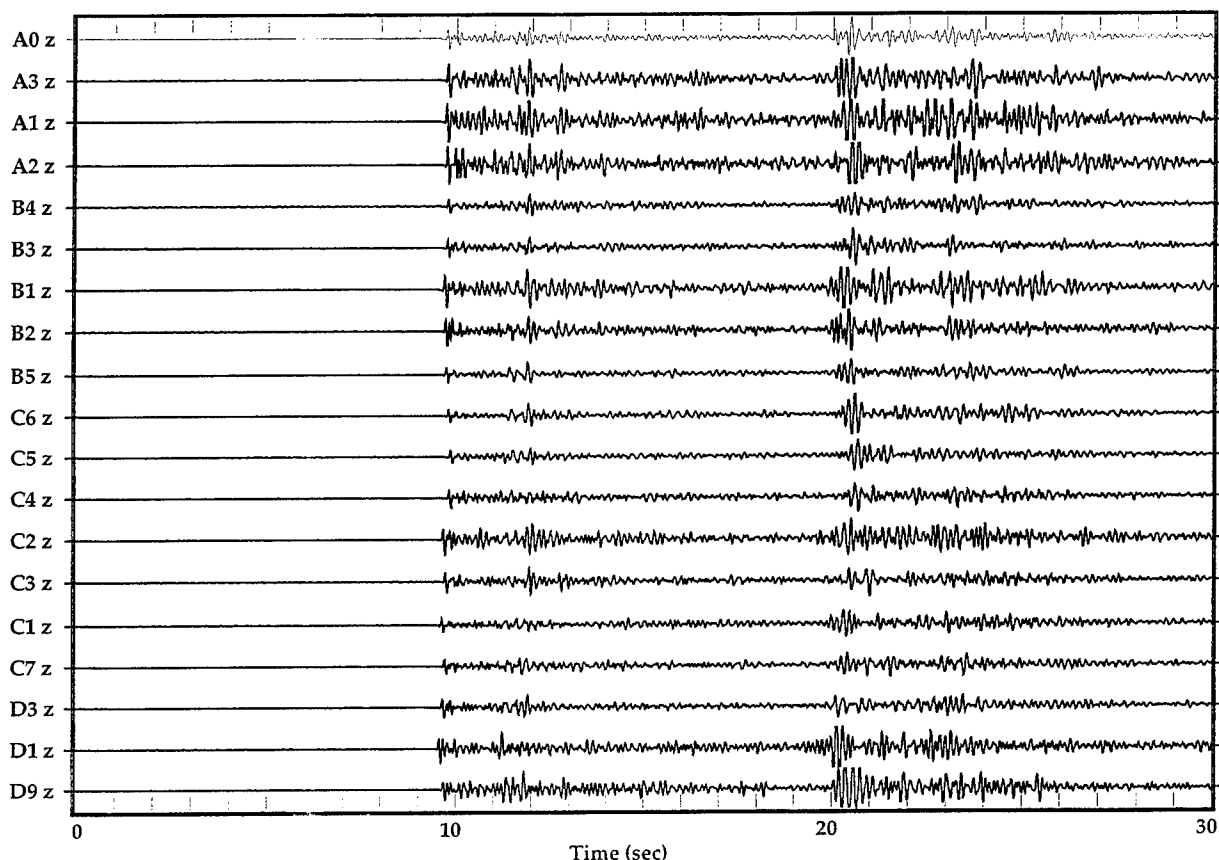


**Figure 13:** Vertical component recordings of an event (91057061432) that occurred roughly 85 km to the northeast of the array. Note the phase arriving 2.25 s after the onset energy. The recordings have been band-passed between 4 and 6 Hz.

P) appears in images of another type of energy (*e.g.* SV) however the degree of contamination is significantly less than in the teleseismic example.

The regional images were calculated by taking advantage of the full PFBA array. To demonstrate the resolution possible with a single 3-C station we have included Figure 10. Steering the station for vertically polarized energy we see that the time-resolution is unchanged; however, the slowness-resolution is poor since with a single station all we have to constrain the direction of propagation is polarization analysis. Surprisingly, a single 3-C station still outperforms a full single (vertical) component array. In Figure 11 we display the SV image calculated by recording the synthetics with a NORESS array. The P-SV conversions have little influence on the vertical components (the particle motion is largely horizontal) and are barely resolved. This image contains uncorrected direct energy (at the origin) and energy due to the P-P bounce at the lower interface (appearing at 30 km).

**4.4.2 Recorded Data.** We have applied our generalized imaging technique to regional and teleseismic events recorded by the 28 station broad-band (.0083 to 40 Hz) 3-C small-aperture PFBA array. During

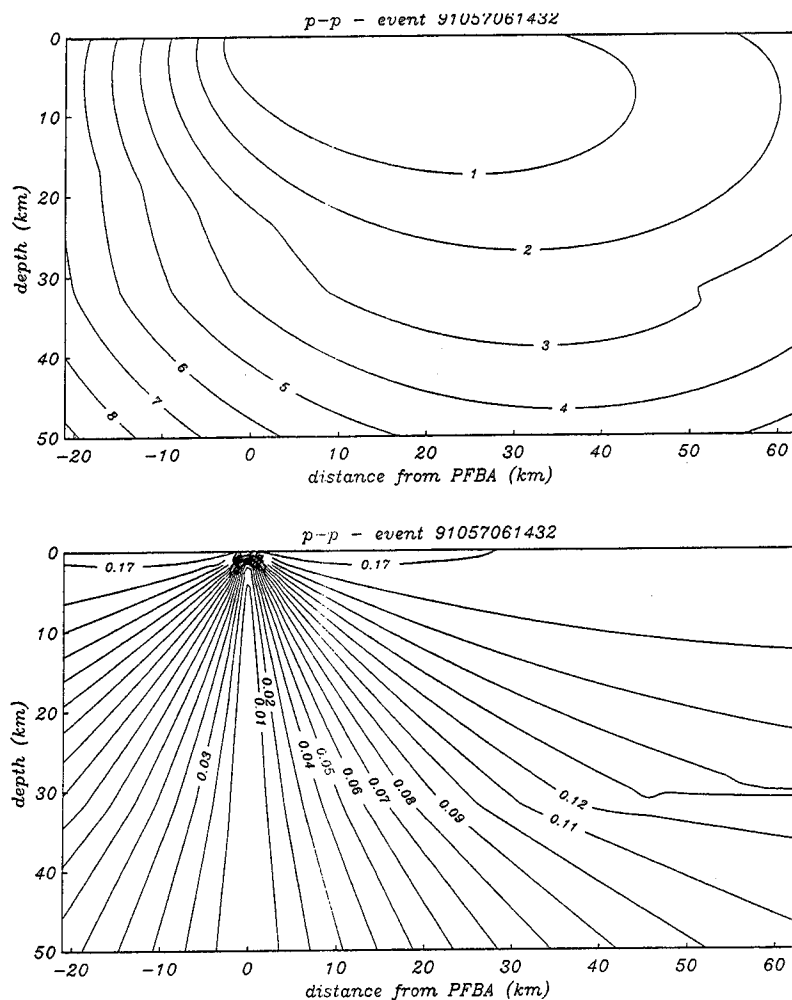


**Figure 14:** Time delay and slowness curves for the event introduced in Figure 13 on a vertical plane passing through the array and bearing  $14^\circ$  east of north. The Earth model used was taken from Scott (1992).

depth of 6 km. The coda contains a significant phase delayed 2.25 s after the P wave onset (figure 13). A  $f-k$  analysis indicates that the onset phase arrives from the azimuth of the event, at a phase velocity of 6.2 km/s while the later phase arrives from a back azimuth of  $14^\circ$  at 12 km/s. In Figure 14 we display the time-delay and slowness surfaces on a vertical plane that passes through the array bearing  $14^\circ$ . Assuming that our velocity model is correct and that this phase has resulted from a single scattering interaction, this figure can be used to predict where the point of re-direction lies. The intersection of the 2.25 s time-delay curve (not highlighted) with the slowness curve corresponding to 1/12 s/km indicates that the energy was redirected at a considerable depth (roughly 30 km) and lies just north of the array. The lower half of Figure 15 contains an image calculated from this event. Although the slowness-resolution is imperfect it is clear that an isolated source exists, as we predicted, at roughly 30 km depth and roughly 20 km to the NNE of the array. The beam correction has been effective - little energy in the image lies at short (less than 1 s) delay times. This result is considerably better than one we would have obtained if the PFBA array contained vertical component stations only. We observe

the winter months of 1991 the array collected triggered (100 sa/s) recordings of 130 local and 140 regional and teleseismic events as well as continuous (20 sa/s) recordings of these, and other smaller, events (see Figure 12). The events are clustered along the most significant faults in the area, the San Andreas (passing just north of the array) and the San Jacinto (just south). Among the events recorded in the triggered mode are a minority that appear to have excited prominent scatterers at the free surface and deeply buried within the crust. As we will see, regions of the local crustal volume that seem to be responsible for particularly large scattered phases bear an interesting relationship to local tectonic features.

One event (which occurred on day 057) occurred 85 km from the array at a back-azimuth of  $35^\circ$  and at a

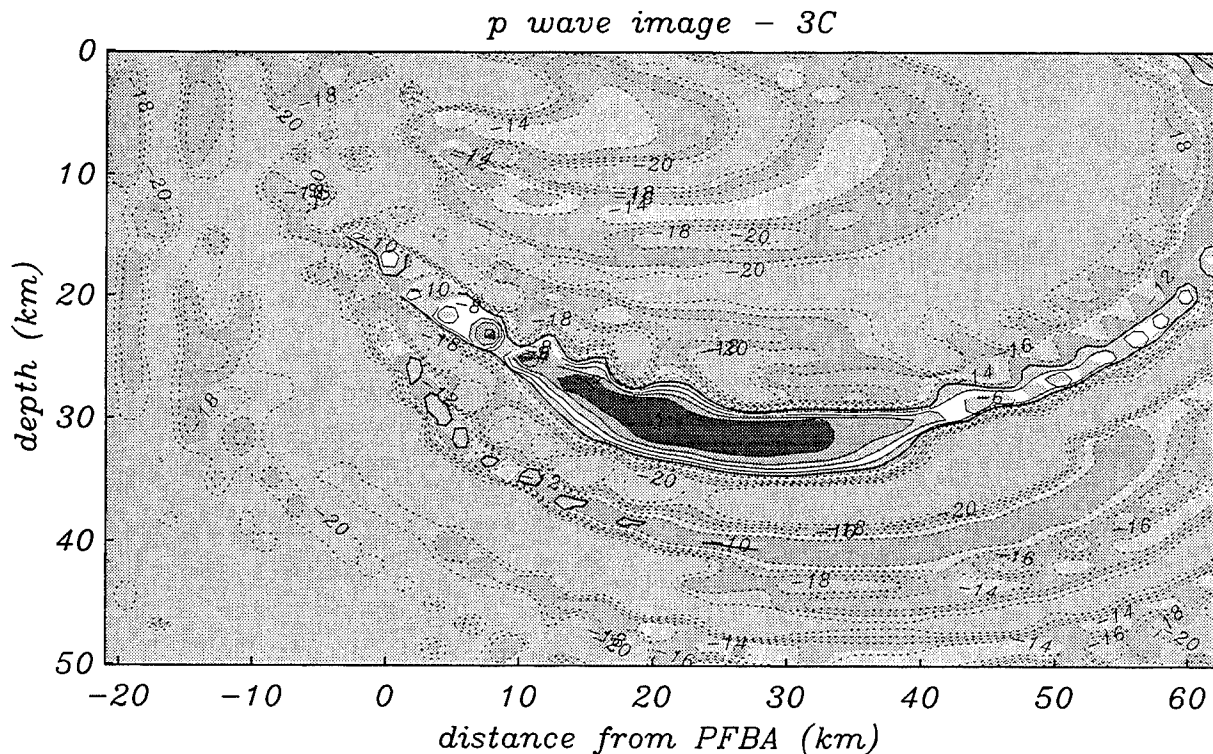
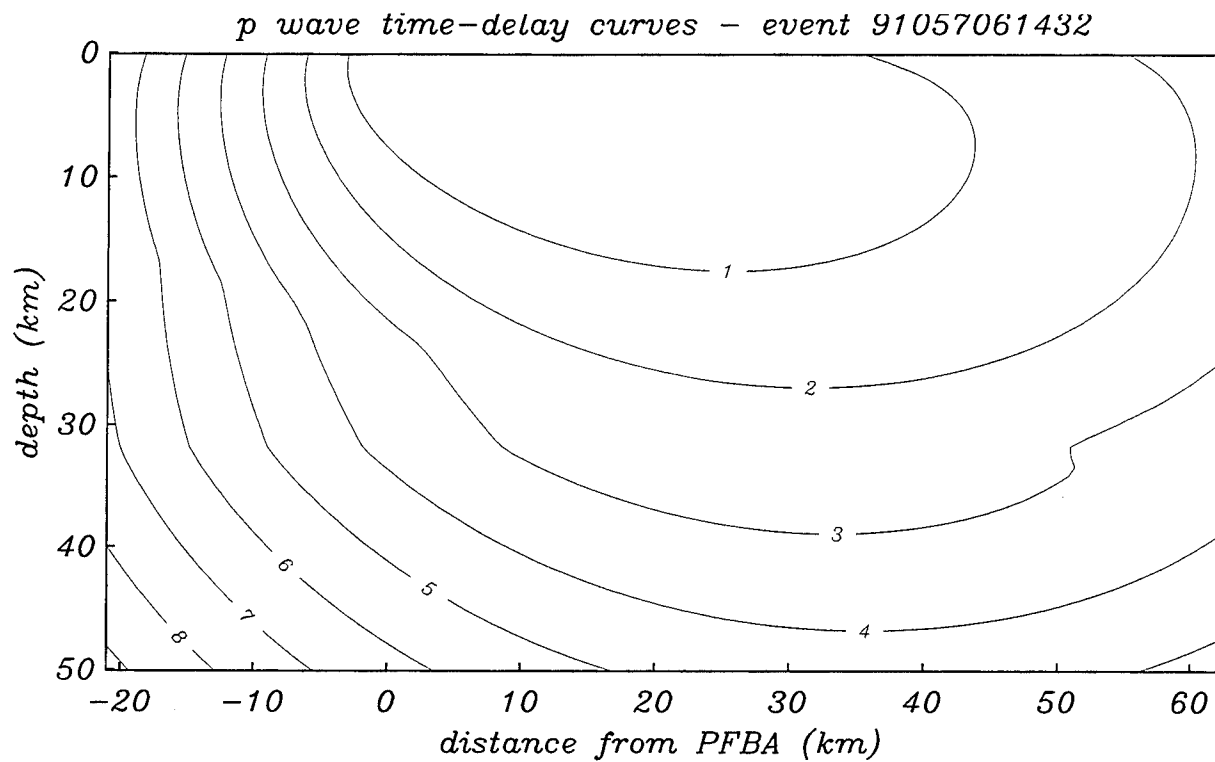


**Figure 15:** 3-Component image calculated using event 91057061432 on the vertical plane introduced in Figure 14. Energy is concentrated at a depth of 30 km roughly 20 to 40 km to the north of the PFBA.

much poorer slowness-resolution and less effective beam correction in the image calculated from the vertical channels (Figure 16). Using the 3-C data, and imaging on a 30 km deep horizontal slice, we see the energy smeared out on elliptical time-delay curves but well confined to a location NNE of the

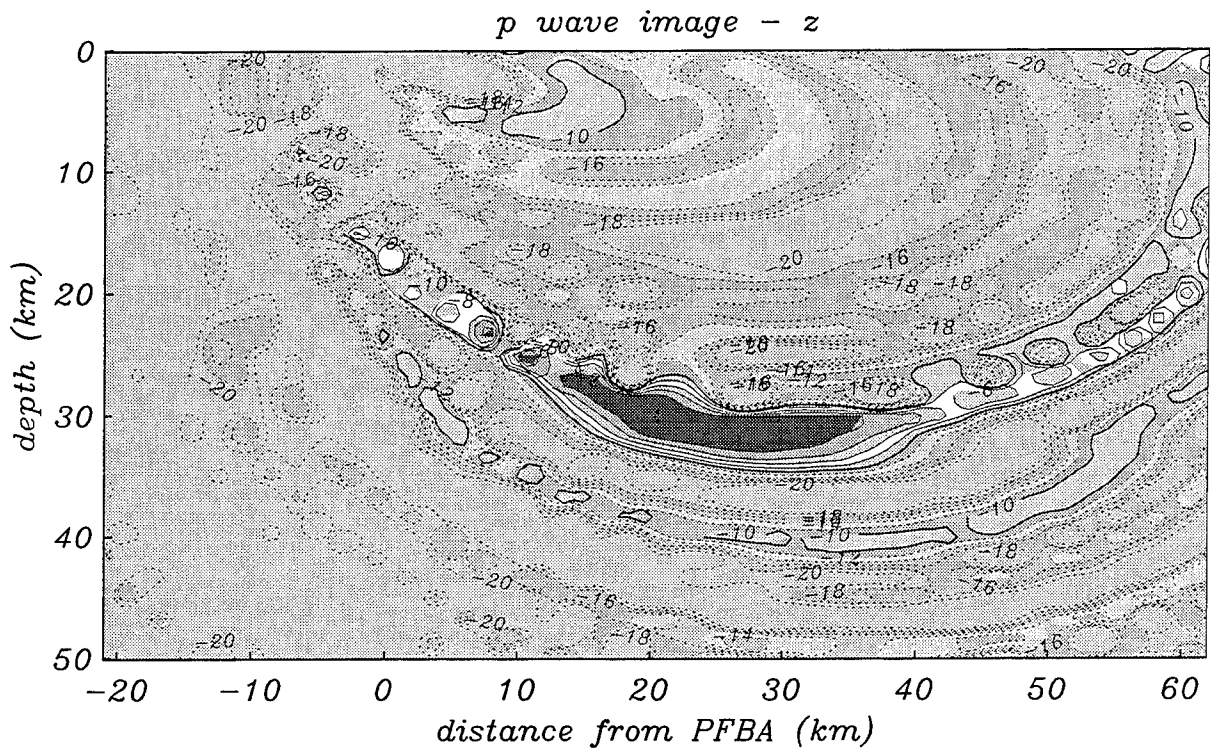
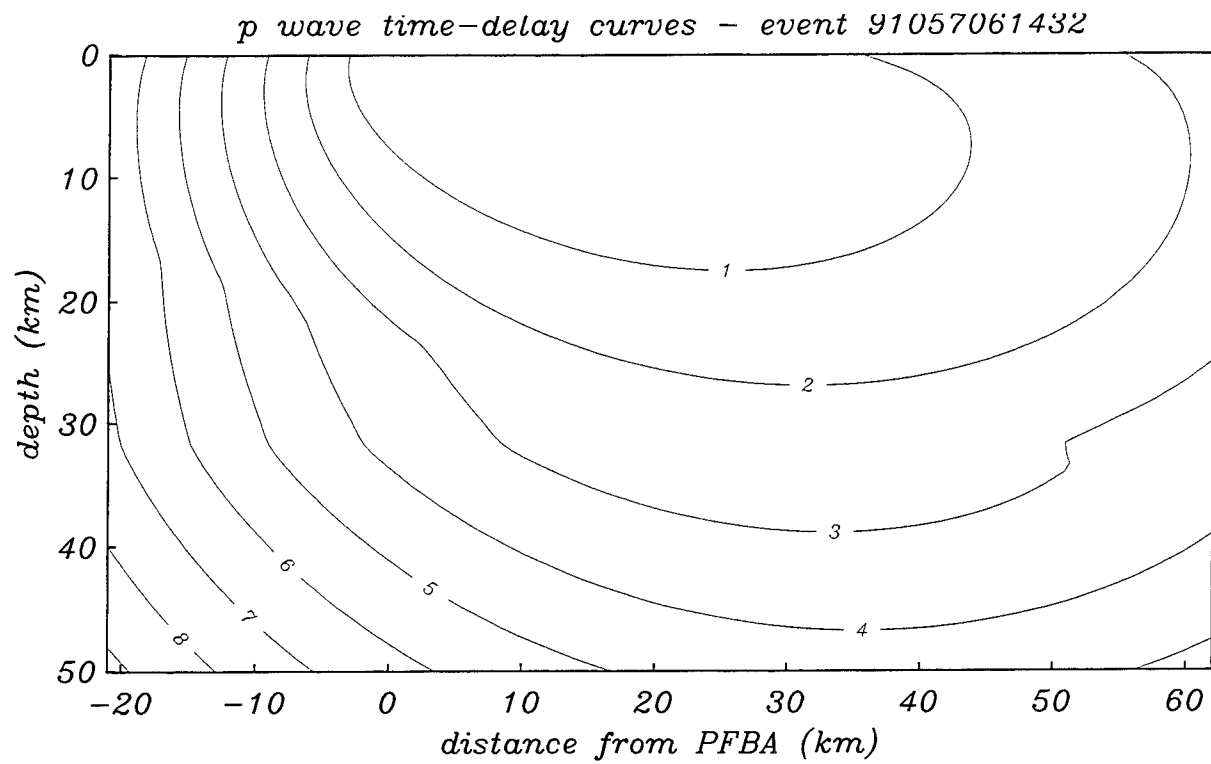


**Figure 16:** This figure is the same as Figure 15 except only the vertical components of the PFBA were used in the imaging. Beam-resolution is inferior to that possible using the full 3-Component array.

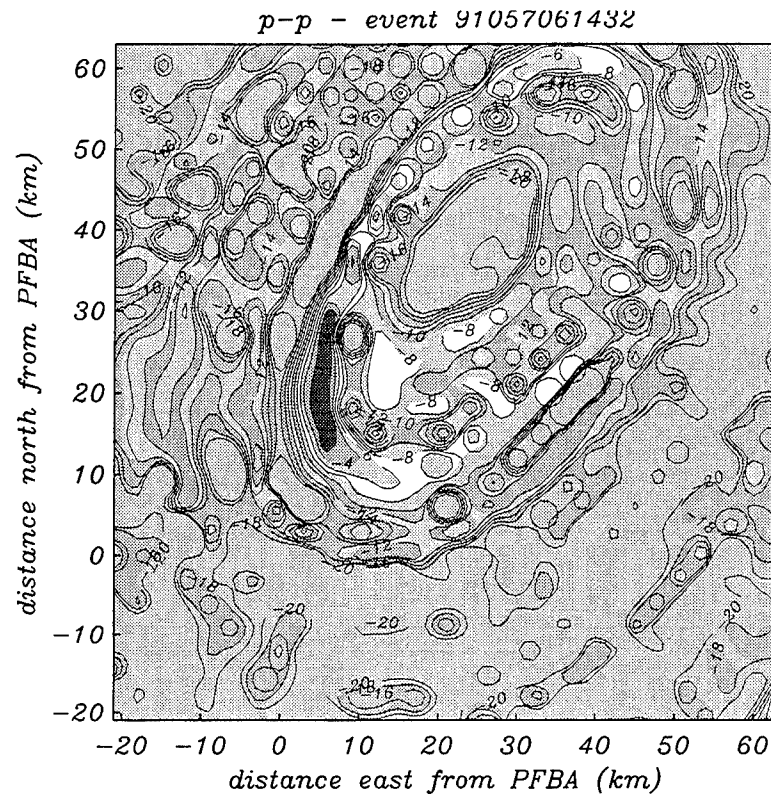


**Figure 17:** A horizontal slice at 30 km depth confirming that the source of the energy is east-northeast of the PFBA.

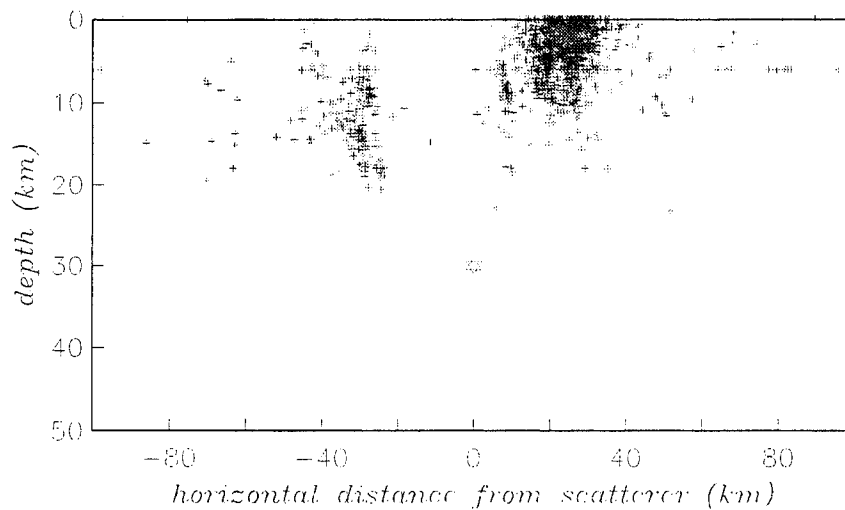


**Figure 18:** Epicenters of events above  $M_l=2.5$  that occurred within 10 km of the plane introduced in Figure 14. The scattering location is represented by the star. This apparent scatterer is well below the seismogenic zone at the northern end of the gap in seismicity.

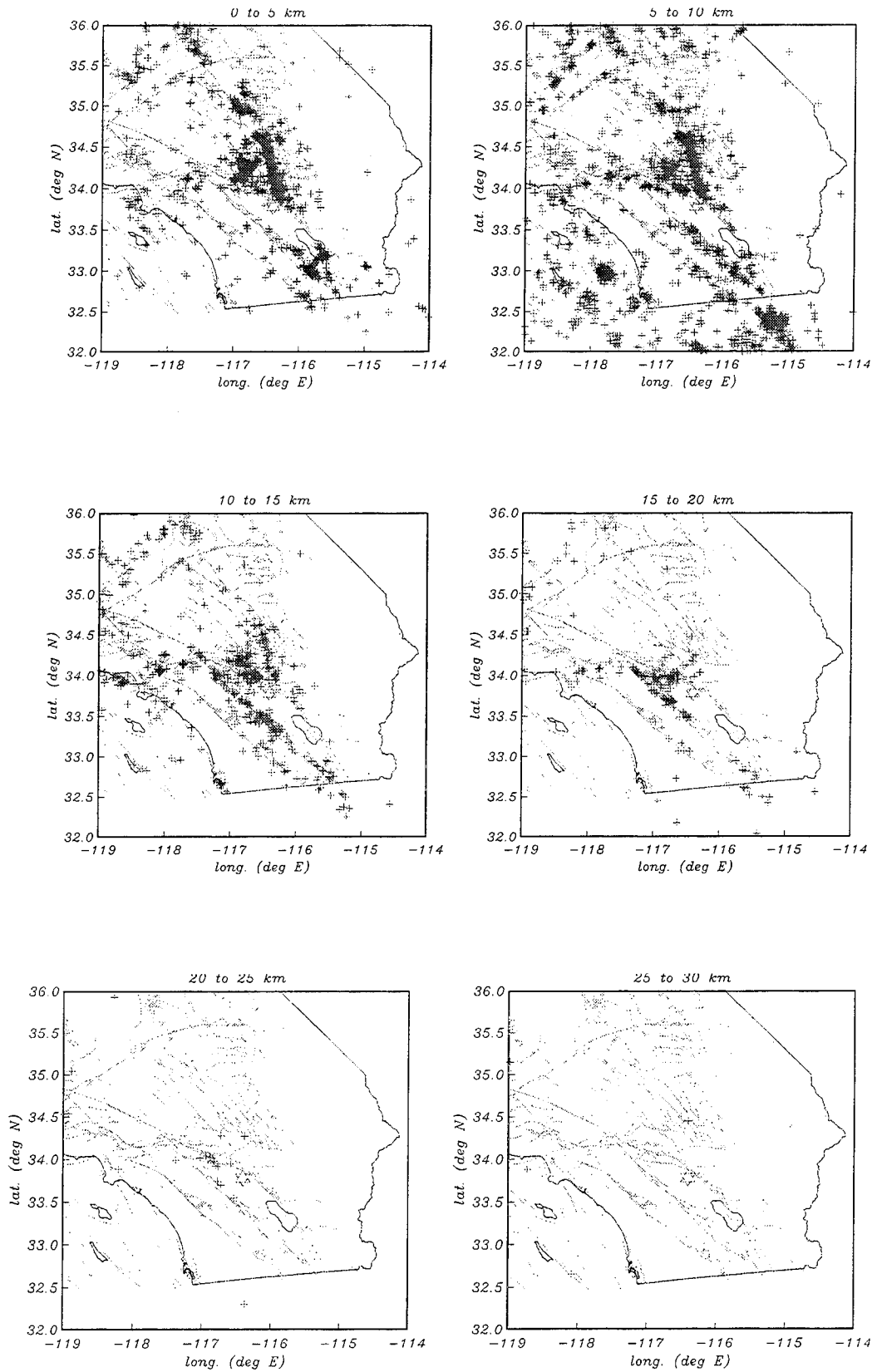


**Figure 19:** Depth slices through southern California seismicity (events with  $M_l$  above 2.5 considered). The deep seismicity (20 to 25 km) is concentrated just northeast of the apparent scatterer.



array (Figure 17). The proximity of this location with the San Andreas fault is intriguing (it is represented by the star in Figure 12). The depth is puzzling, however, since at 30 km it is well below the seismogenic zone (Figure 18). Although it is intriguing that seismicity maps of southern California (Figure 19) indicate that most of the deep events are clustered near this feature we are not yet close to understanding what this scatterer might be due to and what, if any, relationship it bears to the San Andreas fault.

This event is one of a cluster that were recorded by the PFBA array (figure 12). The other events in the cluster recorded in the triggered and continuous modes also, not surprisingly, contained the same phase in the coda. Other large events (the diamonds) appear to have not excited a scatterer at this location indicating that if a scatterer is located here it is highly directional. We will be using the continuous data, which provides tighter spatial coverage, to test the existence of this scatterer and explore, more fully, the nature of its directionality.

#### **4.5 Depth Determination**

The imaging algorithm has been modified so that it can now scan 1-D layered volumes for scatterers excited by regional events. With a few additional modifications it can be used to constrain the depth of the regional events. By treating the near source free-surface bounce as a scatterer and iteratively varying the source depth to bring that energy on to the free surface in the image we can constrain the source depth. This phase of the project is just beginning and we have no results to date.

#### **4.6 The IMS Project**

Currently, we are modifying our time-frequency discrimination code (described by *Hedlin et al.*, 1989 and *Hedlin et al.*, 1990) to make it accessible to the IMS. This involves a significant reorganization of the existing program and writing and debugging existing code to *hook* the main program up with the appropriate tables and relations in the database. We are currently seeking the most appropriate way to get the necessary information from the database into the program to allow it to carry out its discrimination processing. Simply put, we are constructing the custom interface which will be required to connect our program to the Generic Database Interface (GDI).

### **5. IMPORTANT FINDINGS AND CONCLUSIONS**

By analyzing the effects of infinitesimal synthetic scatterers we have gauged image resolution and learned how images of small, symmetrical, scatterers constructed using small-aperture array data might be distorted. We have demonstrated that deploying three orthogonal sensors at each array element, rather than just a single vertical sensor, greatly enhances our ability to resolve scatterers near the array because these components permit us to place much tighter constraints on the direction of propagation of the scattered waves and allow us to separate more effectively the scattered waves from the primary

field. Our analysis of synthetics has demonstrated the degree to which we might expect image resolution to be improved by simultaneously seeking P and S scattered energy.

To date, we have identified a prominent source of scattered energy near PFO using the 28 station PFBA array deployed during 1991. This scatterer appears to be deeply buried within the crust in the vicinity of the San Andreas fault, just north of the observatory. We are currently analyzing a large number of events recorded by this array to refine our view of this apparent scatterer. It appears that the scatterer is highly directional since only a minority of events we have analyzed to date seem to contain phases coming from this location.

## **6. SIGNIFICANT HARDWARE DEVELOPMENT**

none

## **7. IMPLICATIONS FOR FURTHER RESEARCH**

- We will explore, more fully, the apparent scatterer north of PFO. It is not yet known whether only a limited ray geometry leads to scattered phases at the PFBA location. The events recorded in the continuous mode are, generally, smaller than those for which we have triggered records. They provide a denser spatial coverage which might allow us to answer this question.
- The algorithm can, without significant additional alterations, be used to constrain regional event depth using small arrays.

## **8. REFERENCES**

- Aki, K., 1969, Analysis of seismic coda of local earthquakes as scattered waves, *Journal of Geophysical Research*, **74**, 615-631.
- Aki, K. & Chouet, B., 1975, Origin of coda waves: source, attenuation, and scattering effects, *Journal of Geophysical Research*, **80**, 3322-3342.
- Apsel, R.J. & Luco, J.E., 1983, On the Green's functions for a layered half-space, part II, *Bulletin of the Seismological Society of America*, **73**, 931-951.
- Bannister, S.C., Husegye, E.S. & Ruud, B.O., 1990, Teleseismic P coda analyzed by three-component and array techniques: Deterministic location of topographic P-to-Rg scattering near the NORESS array, *Bulletin of the Seismological Society of America*, **80B**, 1969-1986.
- Gupta, I.N., Lynnes, C.S., McElfresh, T.W. & Wagner, R.A., 1990, F-K analysis of NORESS array and single station data to identify sources of near-receiver and near-source scattering, *Bulletin of the Seismological Society of America*, **80B**, 2227-2241.
- Gupta, I.N., Lynnes, C.S. & Wagner, R.A., 1990, Broadband F-K analysis of array data to identify sources of local scattering, *Geophysical Research Letters*, **17**, 183-186.
- Hedlin, M.A.H., Minster, J-B & Orcutt, J.A., 1989, The time-frequency characteristics of quarry blasts

and calibration explosions recorded in Kazakhstan, USSR, *Geophys. J. Int.*, **99**, 109-121.

Hedlin, M.A.H., Minster, J-B & Orcutt, J.A., 1990, An automatic means to discriminate between earthquakes and quarry blasts, *Bull. Seismol Soc. Am.*, **80**, 2143-2160.

Hedlin, M.A.H., Minster, J.B. & Orcutt, J.A., 1991, Beam-stack imaging using a small-aperture array, *Geophysical Research Letters*, **18**, 1771-1774.

Hedlin, M.A.H., Minster, J.B. & Orcutt, J.A., 1994, Resolution of prominent crustal scatterers near the NORESS small aperture array, *Geophysical Journal International*, **119**, 101-115.

Key, F.A., 1967, Signal-generated noise recorded at the Eskdalemuir seismometer array station, *Bulletin of the Seismological Society of America*, **57**, 27-37.

Key, F.A., 1968, Some observations and analysis of signal generated noise, *Geophysical Journal of the Royal Astronomical Society*, **15**, 377-392.

Lay, T., 1987, Analysis of near-source contributions to early P-wave coda for underground explosions. III. Inversion for isotropic Scatterers, *Bulletin of the Seismological Society of America*, **77**, 1767-1783.

Luco, J.E., & Apsel, R.J., 1983, On the Green's functions for a layered half-space, part I, *Bulletin of the Seismological Society of America*, **73**, 909-929.

Lynnes, C.S. & Lay, T., 1989, Inversion of P coda for isotropic scatterers at the Yucca Flat test site, *Bulletin of the Seismological Society of America*, **79**, 790-804.

Richards, P.G., Anderson, D.A. & Simpson, D.W., 1992, A survey of blasting activities in the United States, *Bull. Seismol. Soc. Am.*, **82**, 1416-1433.

Ringdal, Husebye & Dahle, 1975, *Exploitation of Seismograph Networks*, K.G. Beauchamp, Editor, Noordoff-Leiden.

Scott, J., 1992, *Microearthquake studies in the Anza seismic gap*, Ph.D. thesis, University of California, San Diego.

Stump, B., Reamer, S. & Reinke, R., 1988, Temporal and Spatial Source Effects from Near-Surface Explosions, *AFGL/DARPA Seismic. Research. Symposium*, GL-TR-90-0332, ADA230317.

Wallace, T, Blandford, R., Dainty, A., Lacoss, R., Maxion, R., Ryall, A., Stump, B. & Thurber, C., 1992, *Report on the DARPA Seismic Identification Workshop*, May, 1992.

Prof. Thomas Ahrens  
Seismological Lab, 252-21  
Division of Geological & Planetary Sciences  
California Institute of Technology  
Pasadena, CA 91125

Prof. Keiiti Aki  
Center for Earth Sciences  
University of Southern California  
University Park  
Los Angeles, CA 90089-0741

Prof. Shelton Alexander  
Geosciences Department  
403 Deike Building  
The Pennsylvania State University  
University Park, PA 16802

Dr. Thomas C. Bache, Jr.  
Science Applications Int'l Corp.  
10260 Campus Point Drive  
San Diego, CA 92121 (2 copies)

Prof. Muawia Barazangi  
Cornell University  
Institute for the Study of the Continent  
3126 SNEE Hall  
Ithaca, NY 14853

Dr. Douglas R. Baumgardt  
ENSCO, Inc  
5400 Port Royal Road  
Springfield, VA 22151-2388

Dr. T.J. Bennett  
S-CUBED  
A Division of Maxwell Laboratories  
11800 Sunrise Valley Drive, Suite 1212  
Reston, VA 22091

Dr. Robert Blandford  
AFTAC/TT, Center for Seismic Studies  
1300 North 17th Street  
Suite 1450  
Arlington, VA 22209-2308

Dr. Steven Bratt  
ARPA/NMRO  
3701 North Fairfax Drive  
Arlington, VA 22203-1714

Dale Breeding  
U.S. Department of Energy  
Recipient, IS-20, GA-033  
Office of Arms Control  
Washington, DC 20585

Dr. Jerry Carter  
Center for Seismic Studies  
1300 North 17th Street  
Suite 1450  
Arlington, VA 22209-2308

Mr Robert Cockerham  
Arms Control & Disarmament Agency  
320 21st Street North West  
Room 5741  
Washington, DC 20451,

Dr. Zoltan Der  
ENSCO, Inc.  
5400 Port Royal Road  
Springfield, VA 22151-2388

Dr. Stanley K. Dickinson  
AFOSR/NM  
110 Duncan Avenue  
Suite B115  
Bolling AFB, DC

Dr Petr Firbas  
Institute of Physics of the Earth  
Masaryk University Brno  
Jecna 29a  
612 46 Brno, Czech Republic

Dr. Mark D. Fisk  
Mission Research Corporation  
735 State Street  
P.O. Drawer 719  
Santa Barbara, CA 93102

Dr. Cliff Frolich  
Institute of Geophysics  
8701 North Mopac  
Austin, TX 78759

Dr. Holly Given  
IGPP, A-025  
Scripps Institute of Oceanography  
University of California, San Diego  
La Jolla, CA 92093

Dr. Jeffrey W. Given  
SAIC  
10260 Campus Point Drive  
San Diego, CA 92121

Dr. Dale Glover  
Defense Intelligence Agency  
ATTN: ODT-1B  
Washington, DC 20301

Dan N. Hagedorn  
Pacific Northwest Laboratories  
Battelle Boulevard  
Richland, WA 99352

Robert C. Kemerait  
ENSCO, Inc.  
445 Pineda Court  
Melbourne, FL 32940

Dr. James Hannon  
Lawrence Livermore National Laboratory  
P.O. Box 808, L-205  
Livermore, CA 94550

U.S. Dept of Energy  
Max Koontz, NN-20, GA-033  
Office of Research and Develop.  
1000 Independence Avenue  
Washington, DC 20585

Dr. Roger Hansen  
University of Colorado, JSPC  
Campus Box 583  
Boulder, CO 80309

Dr. Richard LaCoss  
MIT Lincoln Laboratory, M-200B  
P.O. Box 73  
Lexington, MA 02173-0073

Prof. David G. Harkrider  
Division of Geological & Planetary Sciences  
California Institute of Technology  
Pasadena, CA 91125

Prof. Charles A. Langston  
Geosciences Department  
403 Deike Building  
The Pennsylvania State University  
University Park, PA 16802

Prof. Danny Harvey  
University of Colorado, JSPC  
Campus Box 583  
Boulder, CO 80309

Jim Lawson, Chief Geophysicist  
Oklahoma Geological Survey  
Oklahoma Geophysical Observatory  
P.O. Box 8  
Leonard, OK 74043-0008

Prof. Donald V. Helmberger  
Division of Geological & Planetary Sciences  
California Institute of Technology  
Pasadena, CA 91125

Prof. Thorne Lay  
Institute of Tectonics  
Earth Science Board  
University of California, Santa Cruz  
Santa Cruz, CA 95064

Prof. Eugene Herrin  
Geophysical Laboratory  
Southern Methodist University  
Dallas, TX 75275

Dr. William Leith  
U.S. Geological Survey  
Mail Stop 928  
Reston, VA 22092

Prof. Robert B. Herrmann  
Department of Earth & Atmospheric Sciences  
St. Louis University  
St. Louis, MO 63156

Mr. James F. Lewkowicz  
Phillips Laboratory/GPE  
29 Randolph Road  
Hanscom AFB, MA 01731-3010( 2 copies)

Prof. Lane R. Johnson  
Seismographic Station  
University of California  
Berkeley, CA 94720

Dr. Gary McCartor  
Department of Physics  
Southern Methodist University  
Dallas, TX 75275

Prof. Thomas H. Jordan  
Department of Earth, Atmospheric &  
Planetary Sciences  
Massachusetts Institute of Technology  
Cambridge, MA 02139

Prof. Thomas V. McEvilly  
Seismographic Station  
University of California  
Berkeley, CA 94720

Dr. Keith L. McLaughlin  
S-CUBED  
A Division of Maxwell Laboratory  
P.O. Box 1620  
La Jolla, CA 92038-1620

Prof. Bernard Minster  
IGPP, A-025  
Scripps Institute of Oceanography  
University of California, San Diego  
La Jolla, CA 92093

Prof. Brian J. Mitchell  
Department of Earth & Atmospheric Sciences  
St. Louis University  
St. Louis, MO 63156

Mr. Jack Murphy  
S-CUBED  
A Division of Maxwell Laboratory  
11800 Sunrise Valley Drive, Suite 1212  
Reston, VA 22091 (2 Copies)

Dr. Keith K. Nakanishi  
Lawrence Livermore National Laboratory  
L-025  
P.O. Box 808  
Livermore, CA 94550

Prof. John A. Orcutt  
IGPP, A-025  
Scripps Institute of Oceanography  
University of California, San Diego  
La Jolla, CA 92093

Dr. Howard Patton  
Lawrence Livermore National Laboratory  
L-025  
P.O. Box 808  
Livermore, CA 94550

Dr. Frank Pilotte  
HQ AFTAC/TT  
1030 South Highway A1A  
Patrick AFB, FL 32925-3002

Dr. Jay J. Pulli  
Radix Systems, Inc.  
201 Perry Parkway  
Gaithersburg, MD 20877

Prof. Paul G. Richards  
Lamont-Doherty Earth Observatory  
of Columbia University  
Palisades, NY 10964

Mr. Wilmer Rivers  
Multimax Inc.  
1441 McCormick Drive  
Landover, MD 20785

Dr. Alan S. Ryall, Jr.  
Lawrence Livermore National Laboratory  
L-025  
P.O. Box 808  
Livermore, CA 94550

Dr. Chandan K. Saikia  
Woodward Clyde- Consultants  
566 El Dorado Street  
Pasadena, CA 91101

Mr. Dogan Seber  
Cornell University  
Inst. for the Study of the Continent  
3130 SNEE Hall  
Ithaca, NY 14853-1504

Secretary of the Air Force  
(SAFRD)  
Washington, DC 20330

Office of the Secretary of Defense  
DDR&E  
Washington, DC 20330

Thomas J. Sereno, Jr.  
Science Application Int'l Corp.  
10260 Campus Point Drive  
San Diego, CA 92121

Dr. Michael Shore  
Defense Nuclear Agency/SPSS  
6801 Telegraph Road  
Alexandria, VA 22310

Prof. David G. Simpson  
IRIS, Inc.  
1616 North Fort Myer Drive  
Suite 1050  
Arlington, VA 22209

Dr. Jeffrey Stevens  
S-CUBED  
A Division of Maxwell Laboratory  
P.O. Box 1620  
La Jolla, CA 92038-1620

Prof. Brian Stump  
Los Alamos National Laboratory  
EES-3  
Mail Stop C-335  
Los Alamos, NM 87545

Prof. Tuncay Taymaz  
Istanbul Technical University  
Dept. of Geophysical Engineering  
Mining Faculty  
Maslak-80626, Istanbul Turkey

Prof. M. Nafi Toksoz  
Earth Resources Lab  
Massachusetts Institute of Technology  
42 Carleton Street  
Cambridge, MA 02142

Dr. Larry Turnbull  
CIA-OSWR/NED  
Washington, DC 20505

Dr. Karl Veith  
EG&G  
5211 Auth Road  
Suite 240  
Suitland, MD 20746

Prof. Terry C. Wallace  
Department of Geosciences  
Building #77  
University of Arizona  
Tuscon, AZ 85721

Dr. William Wortman  
Mission Research Corporation  
8560 Cinderbed Road  
Suite 700  
Newington, VA 22122

ARPA, OASB/Library  
3701 North Fairfax Drive  
Arlington, VA 22203-1714

HQ DNA  
ATTN: Technical Library  
Washington, DC 20305

Defense Technical Information Center  
Cameron Station  
Alexandria, VA 22314 (2 Copies)

TACTEC  
Battelle Memorial Institute  
505 King Avenue  
Columbus, OH 43201 (Final Report)

Phillips Laboratory  
ATTN: GPE  
29 Randolph Road  
Hanscom AFB, MA 01731-3010

Phillips Laboratory  
ATTN: TSML  
5 Wright Street  
Hanscom AFB, MA 01731-3004

Phillips Laboratory  
ATTN: PL/SUL  
3550 Aberdeen Ave SE  
Kirtland, NM 87117-5776 (2 copies)

Dr. Michel Campillo  
Observatoire de Grenoble  
I.R.I.G.M.-B.P. 53  
38041 Grenoble, FRANCE

Dr. Kin Yip Chun  
Geophysics Division  
Physics Department  
University of Toronto  
Ontario, CANADA

Prof. Hans-Peter Harjes  
Institute for Geophysics  
Ruhr University/Bochum  
P.O. Box 102148  
4630 Bochum 1, GERMANY

Prof. Eystein Husebye  
NTNF/NORSAR  
P.O. Box 51  
N-2007 Kjeller, NORWAY

David Jepsen  
Acting Head, Nuclear Monitoring Section  
Bureau of Mineral Resources  
Geology and Geophysics  
G.P.O. Box 378, Canberra, AUSTRALIA

Ms. Eva Johannisson  
Senior Research Officer  
FOA  
S-172 90 Sundbyberg, SWEDEN

Dr. Peter Marshall  
Procurement Executive  
Ministry of Defense  
Blacknest, Brimpton  
Reading FG7-FRS, UNITED KINGDOM

Dr. Bernard Massinon, Dr. Pierre Mechler  
Societe Radiomana  
27 rue Claude Bernard  
75005 Paris, FRANCE (2 Copies)

Dr. Svein Mykkeltveit  
NTNT/NORSAR  
P.O. Box 51  
N-2007 Kjeller, NORWAY (3 Copies)

Dr. Jorg Schlittenhardt  
Federal Institute for Geosciences & Nat'l Res.  
Postfach 510153  
D-30631 Hannover , GERMANY

Dr. Johannes Schweitzer  
Institute of Geophysics  
Ruhr University/Bochum  
P.O. Box 1102148  
4360 Bochum 1, GERMANY

Trust & Verify  
VERTIC  
Carrara House  
20 Embankment Place  
London WC2N 6NN, ENGLAND